

REDUCED ORDER MODELING FOR VAPOR COMPRESSION SYSTEMS VIA  
PROPER ORTHOGONAL DECOMPOSITION

A Thesis

Submitted to the Faculty

of

Purdue University

by

Jiacheng Ma

In Partial Fulfillment of the

Requirements for the Degree

of

Master of Science in Mechanical Engineering

December 2019

Purdue University

West Lafayette, Indiana

**THE PURDUE UNIVERSITY GRADUATE SCHOOL**  
**STATEMENT OF THESIS APPROVAL**

Dr. James E. Braun, Chair

School of Mechanical Engineering

Dr. Donghun Kim

School of Mechanical Engineering

Dr. Neera Jain

School of Mechanical Engineering

**Approved by:**

Dr. Nicole Key

Head of the School Graduate Program

## ACKNOWLEDGMENTS

I would like to express my sincere gratitude to my advisors Dr. James E. Braun and Dr. Donghun Kim, for their insightful guidance and patience throughout my studies. This work would not be possible without their expertise and advice. I am very honored to have the privilege of continuing to work with them.

I would like to thank Dr. Neera Jain for serving on my thesis committee.

I would also like to thank Dr. Daniel Conrad at Hussmann Corporation for offering me a summer internship opportunity. It was an invaluable experience, and I really had fun that summer.

I would like to extend my thanks to colleagues from Ray W. Herrick Laboratories for providing a diverse and inspiring working environment.

I would like to thank the Center for High Performance Buildings at Purdue (CHPB) for sponsoring this research.

I am grateful to Sydni Hair and Chad Hair for accommodating me when I first came to Purdue. Their kind help made it a smooth transition for me.

Finally, I am thankful to my parents for their constant, unconditional support and dedication.

## TABLE OF CONTENTS

	Page
LIST OF TABLES . . . . .	vi
LIST OF FIGURES . . . . .	vii
NOMENCLATURE . . . . .	ix
ABSTRACT . . . . .	xi
1 INTRODUCTION . . . . .	1
1.1 Background and Motivation . . . . .	1
1.2 Dynamic Modeling of Vapor Compression Cycles . . . . .	2
1.3 Model Order Reduction . . . . .	7
1.4 Research Objectives . . . . .	8
1.5 Thesis Organization . . . . .	9
2 MODEL ORDER REDUCTION METHODOLOGIES . . . . .	12
2.1 Introduction . . . . .	12
2.2 Proper Orthogonal Decomposition . . . . .	12
2.2.1 Theory . . . . .	12
2.2.2 Splitting State Space for Coupled Systems . . . . .	16
2.3 Stabilization of POD Reduced Order Models . . . . .	17
2.4 Discrete Empirical Interpolation Method . . . . .	23
3 REDUCED ORDER MODELING FOR VCC . . . . .	28
3.1 Introduction . . . . .	28
3.2 Reformulation of Finite Volume Model . . . . .	28
3.2.1 Governing Equations . . . . .	28
3.2.2 Discretization . . . . .	31
3.3 POD-DEIM Heat Exchanger Models . . . . .	33
3.4 Refrigerant Thermodynamic Properties Evaluation . . . . .	36

	Page
3.5 Cycle Model Implementation . . . . .	40
3.5.1 Object-oriented Modeling with Modelica . . . . .	40
3.5.2 Reduced Cycle Model . . . . .	43
3.5.3 Numerical Treatments . . . . .	45
4 MODEL VALIDATIONS . . . . .	49
4.1 Experimental Facility . . . . .	49
4.2 Model Development . . . . .	50
4.2.1 Compressor . . . . .	50
4.2.2 Expansion valve . . . . .	52
4.2.3 Controller . . . . .	54
4.2.4 Heat Exchangers . . . . .	54
4.2.5 Chiller System . . . . .	63
4.3 Initial Conditions and Control Inputs . . . . .	63
4.4 Load-change Transients . . . . .	64
4.5 Simulation Speed . . . . .	67
5 SUMMARY and RECOMMENDATIONS . . . . .	76
5.1 Summary . . . . .	76
5.2 Recommendations . . . . .	77
REFERENCES . . . . .	79
A Start-up Transients Predictions . . . . .	84

## LIST OF TABLES

Table	Page
4.1 Operating conditions for generating snapshots . . . . .	57
4.2 Reduced order condenser and evaporator models . . . . .	62
4.3 Simulation speed comparison . . . . .	71

## LIST OF FIGURES

Figure	Page
1.1 Finite volume heat exchanger model. . . . .	3
1.2 Moving boundary heat exchanger model. . . . .	5
1.3 An illustration of model order reduction. . . . .	8
2.1 Projection of states vector onto a basis. . . . .	14
3.1 Staggered grid for discretization on the refrigerant side . . . . .	31
3.2 Control volume object of the reformulated HX model. . . . .	32
3.3 Nonlinear model order reduction framework. . . . .	37
3.4 Calculation Bounds of R134a on P-h diagram . . . . .	38
3.5 Calculation domain of R134a on $\rho - u$ diagram . . . . .	39
3.6 Neural Network architecture for calculating thermodynamic properties . . . . .	40
3.7 Vapor compression system in TIL library. . . . .	42
3.8 Generating reduced order VCC model. . . . .	44
3.9 Smoothing a step change by a polynomial function. . . . .	46
4.1 Schematic of chiller system. . . . .	49
4.2 Refrigerant flow schematic. . . . .	50
4.3 Refrigerant single-phase heat transfer coefficient as a function of flow rate and temperature . . . . .	55
4.4 Water heat transfer coefficient as a function of flow rate and temperature . . . . .	56
4.5 Density snapshots energy ratio. . . . .	59
4.6 Internal energy snapshots energy ratio. . . . .	59
4.7 Mass flow rate snapshots energy ratio. . . . .	60
4.8 Temperatures snapshots energy ratio. . . . .	60
4.9 Refrigerant energy balances snapshots energy ratio. . . . .	61
4.10 Refrigerant momentum balances snapshots energy ratio. . . . .	61

Figure	Page
4.11 Tube and water energy balances snapshots energy ratio. . . . .	62
4.12 chiller system model implemented in Dymola. . . . .	64
4.13 Control inputs of water inlet temperatures and set point temperature. . . . .	65
4.14 Control inputs of water mass flow rates. . . . .	66
4.15 Condensing and evaporating pressures. . . . .	68
4.16 Condenser and evaporator water exit temperatures. . . . .	68
4.17 Motor Power. . . . .	69
4.18 Condenser load. . . . .	69
4.19 Evaporator load. . . . .	70
4.20 Liquid refrigerant mass flow rate. . . . .	70
4.21 Normalized Error Residual. . . . .	71
4.22 Steady-state condensing and evaporating pressures. . . . .	72
4.23 Steady-state exit water temperatures. . . . .	72
4.24 Steady-state evaporator loads. . . . .	73
4.25 Density of R134a at 8 bar. . . . .	74
4.26 Density derivatives. . . . .	75
A.1 Cycle boundary conditions: heat exchanger water mass flow rates and inlet temperatures. . . . .	84
A.2 Condensing and evaporating pressures . . . . .	85
A.3 Condenser and evaporator water exit temperatures . . . . .	86
A.4 Condenser Load. . . . .	86
A.5 Evaporator Load. . . . .	87

## NOMENCLATURE

**Symbols**

$A$	Flow area [m <sup>2</sup> ]
$a$	Reduced order states
$C_p$	Specific heat [kJ/(kgC)]
$h$	Enthalpy [kJ/kg]
$I$	Momentum [kg · m/s <sup>2</sup> ]
$L$	Tube length [m]
$M$	Mass [kg]
$\dot{m}$	Mass flow rate [kg/s]
$P$	Pressure [kPa]
$P_{mo}$	Motor power [kW]
$\dot{Q}$	Heat transfer rate [kW]
RLA	Rated load Amps
RTF	Real time factor [-]
$T$	Temperature [C]
$u$	Internal energy [kJ/kg]
$V$	Volume [m <sup>3</sup> ]
$\dot{V}$	Volume flow rate [m <sup>3</sup> /s]
$v$	Velocity [m/s]
$W_p$	Polytropic work [kJ/kg]
$x$	Dynamic states
$x$	Refrigerant quality [-]

**Greek letters**

$\alpha$	Heat transfer coefficient [kW/(m <sup>2</sup> C)]
----------	---

$\gamma$	Mass flow rate correction factor [-]
$\eta$	Efficiency [-]
$\mu$	Frictional factor
$\rho$	Density [kg/m <sup>3</sup> ]

**Subscript**

$b$	Bulb
$c$	Condenser
$cl$	Cooling line
$e$	Evaporator
$i$	Inlet
$out$	Outlet
$r$	Refrigerant
$t$	Tube
$v$	Valve
$w$	Water

## ABSTRACT

Ma, Jiacheng M.S.M.E, Purdue University, December 2019. Reduced Order Modeling for Vapor Compression Systems via Proper Orthogonal Decomposition. Major Professor: James E. Braun.

Dynamic modeling of Vapor Compression Cycles (VCC) is particularly important for designing and evaluating controls and fault detection and diagnosis (FDD) algorithms. As a result, transient modeling of VCCs has become an active area of research over the past two decades. Although a number of tools have been developed, the computational requirements for dynamic VCC simulations are still significant. A computationally efficient but accurate modeling approach is critically important to accelerate the design and assessment of control and FDD algorithms where a number of iterations with a variety of test input signals are required. Typically, the dynamics of compressors and expansion devices evolve on an order of magnitude faster than those of heat exchangers (HX) within VCC systems. As a result, most dynamic modeling efforts have focused on heat exchanger models. The switched moving boundary (SMB) method, which segments a heat exchanger depending on thermodynamic phase of the refrigerant, i.e. subcooled liquid, two-phase and superheated vapor, and moves control volumes as the length of each phase changes, can reduce the computation time compared with the finite volume (FV) method by solving fewer equations due to a smaller set of control volumes. Despite the computational benefit of the SMB, there is a well-known numerical issue associated with switching the model representations when a phase zone disappears or reappears inside of a heat exchanger. More importantly, the computational load is still challenging for many practical VCC systems. This thesis proposes an approach applying nonlinear model order reduction (MOR) methods to dynamic heat exchanger models to generate reduced order HX models,

and then to couple them to quasi-static models of other VCC components to complete a reduced order VCC model. To enable the use of nonlinear model reduction techniques, a reformulated FV model is developed for matching the baseline MOR model structure, by using different pairs of thermodynamic states with some appropriate assumptions. Then a rigorous nonlinear model order reduction framework based on Proper Orthogonal Decomposition (POD) and the Discrete Empirical Interpolation Method (DEIM) is developed to generate reduced order HX models.

The proposed reduced order modeling approach is implemented within a complete VCC model. Reduced order HX models are constructed for a centrifugal chiller test-stand at Herrick Labs, Purdue University, and are integrated with quasi-static models of compressor and expansion valve to form the complete cycle. The reduced cycle model is simulated in the Modelica-based platform to predict load-change transients, and is compared with measurements. The validation results indicate that the reduced order model executes 200 times faster than real time with negligible prediction errors.

# 1. INTRODUCTION

## 1.1 Background and Motivation

Dynamic modeling of Vapor Compression Cycles (VCC) has become an active area of research over the past two decades. Developing reliable and computationally efficient transient modeling approaches is particularly important for advancing design and operation of modern HVAC&R (Heating, Ventilation, Air-Conditioning and Refrigeration) systems. In particular, understanding the complicated thermo-fluid behaviors inside VCC equipment and capturing their nonlinear dynamics are useful for designing and evaluating controls and fault detection and diagnosis (FDD) algorithms. Previous studies have shown that advanced control and FDD algorithms built upon dynamic models can lead to better performance and higher efficiency for residential air conditioner and building HVAC applications [1–3]. In control design, experimental evaluation of control algorithms is costly and inefficient. Therefore dynamic models that can capture the relevant dynamics of the system are necessary. In addition, fault detection and diagnosis method could be easily evaluated using dynamic models, thereby saving testing time and effort.

Although a number of tools have been developed for dynamic VCC simulations, the computational requirements are still significant, due to the nature of solving nonlinear differential equations. The computer execution speed of a transient model depends on a number of factors, including the dimensions of equations to be solved, the numerical methods, the accuracy requirements, etc. Typically, the dynamics of compressors and expansion devices evolve an order of magnitude faster than those of heat exchangers within VCC systems. As a result, most dynamic modeling efforts have focused on heat exchanger models over the past few decades. The two dominant approaches, the finite volume (FV) and moving boundary (MB) methods, have

been widely studied, and reported to successfully capture the complex thermo-fluid behavior within heat exchangers [4–6]. Generally, the FV model is much simpler to derive and implement, and has advantages of robustness and flexibility over the MB approach. The MB model is found to have faster simulation speed, but there’s a well-known numerical issue associated with model representation switches [7]. An overview of FV and MB modeling approaches, and detailed comparisons between them are presented in the next section. More importantly, the computational requirements are still challenging for many practical VCC systems, and this issue brings difficulties in designing and evaluating many advanced control techniques. A computationally efficient but accurate modeling approach is important in accelerating the design and assessment of control and FDD algorithms where a number of iterations with a variety of test inputs signals are needed.

## 1.2 Dynamic Modeling of Vapor Compression Cycles

Vapor compression cycles used in refrigeration, air conditioning, and heat pump applications generally consist of four major components: condenser, evaporator, compressor and expansion device. In transient simulations, system component models can be divided into two categories, dynamic models of heat exchangers describing the refrigerant flow and heat transfer behaviors, and quasi-static models of the compressor and expansion device for mass flow rates calculation without considering the refrigerant mass storage. Most dynamic modeling efforts for heat exchangers can be classified as either a finite volume or moving boundary approach. The fundamental difference between them is the discretization strategy that is utilized to solve the conservation equations. The finite volume method divides the heat exchanger into a fixed number of equally sized control volumes, and the governing equations are integrated over each of them. The refrigerant properties are lumped in each volume and may switch between different phase regions (subcooled, two-phase, superheated), as the states and control inputs change. For example, Fig. 1.1 depicts a finite volume con-

denser model. The finite volume heat exchanger models can achieve different levels of fidelity based on the number of control volumes resulting from the spatial discretization. It is capable of modeling the thermo-fluid behavior in a detailed manner and high prediction accuracy, with a sufficient discretization level. However, using a large number of control volumes results in a large set of governing equations, and a high order dynamic model. MacArthur [8] presented a detailed mathematical model for describing transients in heat pumps based on the finite volume method. Gruhle and Isermann [9] used a discretized model of the evaporator for model-based design of a PI valve control strategy, but no validation was presented. Bendapudi [10] presented numerical studies on the effect of spatial discretization level. The finite volume heat exchanger models were developed to predict transients in a chiller system. It was demonstrated that increasing the number of control volumes improves accuracy, but beyond a certain number of volumes, the model achieved mesh independence, and further increases in discretization gave negligible accuracy improvement. It was found that the prediction accuracy remained unchanged up to 15 control volumes for a flooded condenser and evaporator. Tso et al. [11] used finite difference discretization to study dynamic behavior of an evaporator under frosting conditions. Zhang et al. [12] compared different forms of momentum balances in a finite volume model. Numerical studies revealed that including the momentum balances was not critical for predicting large transients.

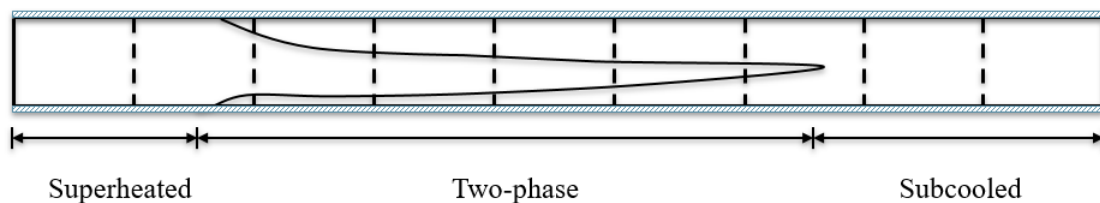


Fig. 1.1. Finite volume heat exchanger model.

The moving boundary method segments heat exchangers depending on thermodynamic phase of the refrigerant, i.e. subcooled (SC), two-phase (TP), and superheated

(SH), and moves control volumes as the length of each phase section changes. Consequently, the MB model solves fewer equations due to fewer control volumes. Fig 1.2 depicts a moving boundary condenser model. Similar to the finite volume method, each control volume is still analyzed with a lumped parameter approach. The lumped properties are calculated with the assumption of a linear enthalpy profile along each volume. The difference is that the size of volumes can vary with time as the phase flow length changes. Corresponding to different operating conditions of the heat exchanger, a phase zone could completely disappear or reappear, which results in a changeable model dimension, and case-by-case mathematical description. Thus the MB model should be capable of switching between different model representations. Such methods are often referred to as switched moving boundary (SMB) models. In case of the highest model order, the heat exchanger is lumped into three zones. The dimension of the resulting system is much smaller than the FV method, since the total number of conservation equations to be solved is proportional to the number of control volumes. Because of the lower state dimensionality and reasonable prediction accuracy, the MB has been extensively utilized for control applications for VCC [13–15]. MB formulations have been derived and advanced in a series of previous work. Grald and MacArthur [13] developed a two-zone MB formulation for an evaporator, and incorporated a void fraction model for the two-phase zone. A comparison with a FV model demonstrated comparable accuracy of the MB model with a lower computational cost. He [14] explored MB models for both condenser and evaporator. The evaporator dynamics were lumped into two zones, and the condenser dynamics into three zones. The model was proven to be useful for a feedback control design. Willatzen et al. [16] formulated a set of heat exchanger MB models for three-zone, two-zone, one-zone modes for an evaporator. A switching algorithm that monitors enthalpy and selects an appropriate mode was presented. Jensen and Tummescheit [17] tested a virtually identical three-zone MB model for an evaporator of an Organic Rankine Cycle. Zhang and Zhang [18] investigated the MB evaporator model employing a time variant void fraction model. The model was able to switch

between TP and TP-SH mode when the superheated region was used to trigger switch events. Bendapudi et al. [5] extended the MB formulations for more general phase combinations, e.g. SH, SH-TP and SH-TP-SC for condenser and TP, TP-SH for evaporator, and applied the enthalpy-based rules for mode switching. The main challenge within the model structures is in the mismatch of the number of state dimensions for different modes. McKinley and Alleyne [19] provided a method that can systematically overcome the mismatch problem by introducing pseudo-state variables. In the methodology, dynamic states associated with inactive zones are evaluated by pseudo state equations when a phase zone disappears. This provides reasonable initial conditions for the states when the zone reappears.

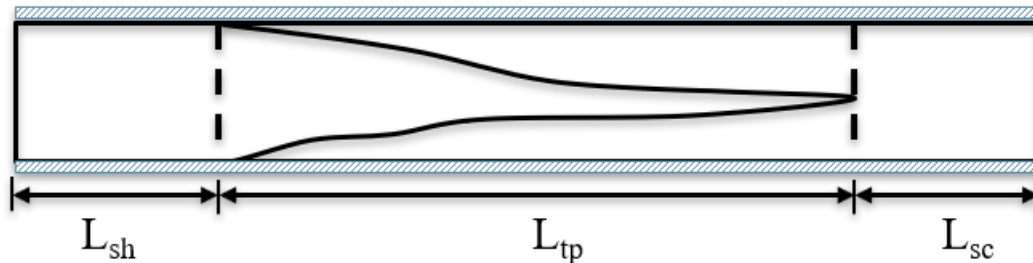


Fig. 1.2. Moving boundary heat exchanger model.

Some previous work has been devoted to comparisons between the FV and MB approaches. Bendapud et al. [5] presented comparative studies of shell-and-tube heat exchanger dynamic models using both FV and MB methods. The FV formulation was found to be more robust through start-up and load-change transients, but executed slower. The MB model executed three time faster than the FV while maintaining nearly identical accuracy, but the start-up stability was more sensitive to the boundary conditions profile. Rasmussen [20] compared simulation results of FV and switched MB models in response to step changes in expansion valve and compressor speed. No comparison to experimental results is provided. It is stated that both models were capable of handling start-up and shut-down transients (e.g. a loss of evaporator superheat), and predictions of FV and switched MB models are

indistinguishable. Pangborn et al. [4] challenged the conventional tradeoff between computational speed and accuracy when comparing the FV and MB approaches. It is stated that by integrating the mean void fraction models for the two-phase cell in the MB heat exchanger model, it is capable of achieving similar levels of accuracy as the FV model. A new view was proposed that computational load and flexibility are the true tradeoff of FV and MB approaches. The switched MB approach can execute much faster in simulation than the FV approach, and there is little difference between the two in the achievable accuracy relative to experimental data. Though the FV approach executes slower, it does have advantages that the model is much simpler to derive and implement than the MB model due to complexity of changeable control volume lengths and the need to incorporate a mean void fraction model. It is flexible to use the FV approach for achieving different levels of fidelity as a tradeoff with simulation speed by modifying the number of control volumes into which the heat exchanger is discretized. Furthermore, the FV approach is found to be more useful when detailed heat exchanger states are desired. For example, it is useful to have access to the tube material temperatures calculated by the FV model in modeling frost formation on the surface of heat exchangers.

Despite a long history and a large number of investigations and applications of the MB method, there is still a significant challenge in designing a general and reliable switching algorithm for smooth transitions between the case-by-case model representations. As mentioned in [5], the MB formulation is less robust and more sensitive to a shape of boundary conditions compared with the FV when a heat exchanger undergoes several mode switches during a very short time period, e.g. start-up. Qiao et al. [7] discussed that mode switching is on a case-by-case basis. The mode switching sequence is not universally valid, and only works for the specified cases.

The robustness issue of a switched MB model is mainly due to an event trigger in switching model representations. All approaches are based on IF-THEN rules, and hence contain potential numerical issues such as a high stiffness, chattering near

transition points, additional computation to overcome the high stiffness, and possible numerical instability due to inherent discontinuities of IF-THEN rules.

Recently, dynamic modeling of HVAC equipment models has been advanced by object-oriented and equation-based modeling languages (Modelica in particular). Due to the nature of high nonlinearity, multi-domain scale of HVAC models, it is challenging to implement simulation and control in conventional modeling programs (e.g. C++) and platforms (e.g. Simulink). The Modelica-based modeling platforms, such as Dymola and MapleSim, address these issues by introducing the concept of acausal modeling, and have attracted enormous attention from both academia and industry [21–23].

### 1.3 Model Order Reduction

In many engineering applications, it is often required to run real-time simulations that solve systems of differential equations describing the physical phenomena of interest. When the governing partial differential equations (PDEs) are discretized by grid-based numerical methods, the dimension of the resulting systems can become extremely large in order to provide satisfactory approximating accuracy. However, a large dimensionality of high-fidelity computational models makes them CPU intensive, and therefore impractical or even infeasible for real-time simulations in optimization, optimal control, and design.

Model order reduction (MOR) techniques can be used to reduce the computational complexity and simulation time of large-scale dynamical systems by producing reduced order models (ROMs) with much smaller dimension, but capable of capturing dominant characteristics of the original models. A common model reduction approach is based on projecting a high-fidelity model onto a low dimensional subspace, which is expected to contain essential information of the corresponding solution space, and constrain the resulting residual of the governing equations. The low-dimension subspace is often referred to as the reduced order basis (ROB), which consists of a set

of basis functions (vectors). Fig 1.3 illustrates the idea of MOR. For a general high-fidelity dynamical system arising from classical discretization schemes, e.g. finite difference, finite element, or finite volume methods, model reduction seeks a reduced system with reduced dynamic states whose dimension  $N_r$  is much smaller than the original system, as well as reduced functions  $f_r(\cdot)$  and  $g_r(\cdot)$ , that can preserve the input-output responses of the original system.

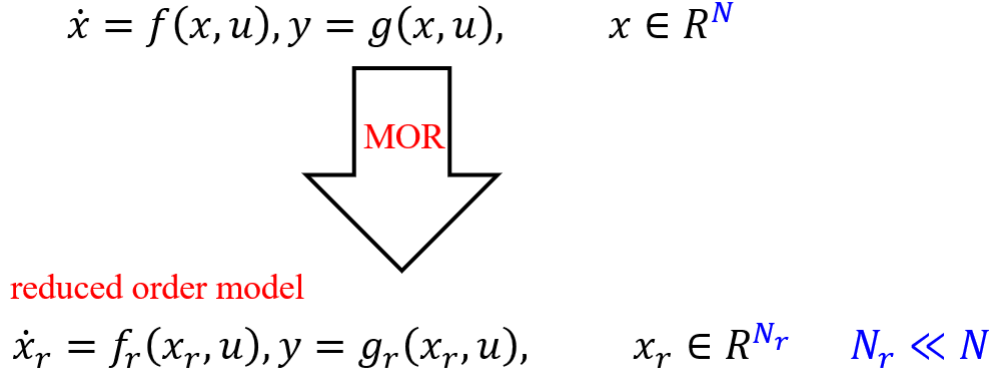


Fig. 1.3. An illustration of model order reduction.

Among the various techniques for obtaining a reduced order basis, Proper Orthogonal Decomposition (POD) constructs a reduced basis that is optimal in the sense that a certain projection error is minimized, and it is applicable to general nonlinear systems. The POD method is therefore adopted in this work.

#### 1.4 Research Objectives

Based on the literature review of dynamic modeling approaches for vapor compression systems, it is still challenging to utilize the current simulation tools for control design and fault detection purposes. Since the dynamics of heat exchangers have the greatest effect on the overall transient behavior of the system, developing heat exchanger models is an important step to advance simulation programs. As described earlier, two popular approaches, the finite volume and the moving boundary,

yield fundamental differences. The moving boundary approach has been more often adopted for control design in the literature [15,24–26], due to its low order model structure, and faster execution in simulation. However, the numerical issue associated with model switching limits the application of the MB approach under certain conditions, and it is more difficult to extend the MB approach to various heat exchanger types and geometries, as acknowledged in [20]. Improving robustness of the switched MB method is a remaining issue that deserves more effort in the near future. The FV approach can accurately capture detailed dynamics, and is intended to handle “hard” transients where the switched MB may potentially fail. These features of the FV model are obtained at the expense of high computational load, which prevents its application in control and FDD. The objective of this work is to develop and validate a fast and robust dynamic modeling approach for VCC systems that can be directly used for control and FDD applications. Based on the flexibility and robustness advantages, the FV approach is therefore used here as a starting point. Then nonlinear model order reduction methods are applied to the FV models to generate reduced order heat exchanger models, to overcome the computational inefficiency of the FV approach. Finally they are coupled to quasi-static models of other VCC components to complete a reduced order VCC model. The reduced order system model will be validated with available measurements, and the overall accuracy and computational speed will be compared with a conventional dynamic VCC system model.

## 1.5 Thesis Organization

This chapter has described motivation of this work, followed by a review of dynamic modeling for vapor compression systems, and challenges in the existing modeling approaches. A high-level overview of model order reduction was provided, as well as the research objectives.

Chapter 2 describes the methodologies that are used in this work to generate reduced order heat exchanger models. The model reduction method, Proper Orthog-

onal Decomposition (POD) is described, and the solution is derived. After that, a splitting scheme for coupled nonlinear systems is introduced. POD reduced order models, in general, are not guaranteed to preserve the stability property of the original high-fidelity models. A sufficient condition for preserving stability is described. After that, a stabilization algorithm motivated by the condition is discussed. However, this method solely operates on the full order model as a *prior*. It is challenging to find the optimal value due to the high dimensionality of the full order model, and it is not straightforward to implement with the splitting scheme. Therefore, another stabilization method operating on the reduced order basis is described. The method is more promising because of its flexibility in forming reduced order models. The POD reduced order model is not efficient for nonlinear dynamical systems. Though the number of dynamic states is reduced, the computational complexity of evaluating nonlinear functions remains. To overcome this issue, techniques for approximating nonlinear functions should be used in conjunction with the POD model reduction method to further improve dimension reduction efficiency. A discrete empirical interpolation method (DEIM) is described to address this nonlinear model order reduction issue.

Chapter 3 describes the application of model order reduction methods to vapor compression cycles. To enable the use of nonlinear model reduction techniques, a reformulated finite volume heat exchanger model utilizing refrigerant density, internal energy, and interface mass flow rates as states is developed. Then application of the POD-DEIM method on the reformulated model is described, and procedures to generate POD-DEIM reduced order models are summarized. Calculations of refrigerant thermodynamic properties play an important role in transient VCC simulations. A fast thermodynamic properties evaluation scheme based on Neural Networks is introduced. After that, the implementation of the reduced order VCC model in the Modelica-based simulation environment is described. An overview of dynamic VCC modeling using Modelica is presented. Then implementation of the proposed reduced

order modeling approach in the Modelica modeling language is described. Additionally, numerical treatments for improving model robustness are introduced.

Chapter 4 presents validations of the reduced order modeling approach for a centrifugal chiller system. The experimental facility is described, followed by models of each component. Then initial conditions and control inputs used in simulation are described. The reduced order cycle model is simulated to predict load-change transients of the chiller system, and compared with the measurements. Finally, simulation speed comparisons with the standard FV model and the reformulated full order model are presented.

The work presented in this thesis is summarized in Chapter 5, and recommendations for further studies are discussed.

## 2. MODEL ORDER REDUCTION METHODOLOGIES

### 2.1 Introduction

This chapter presents the model order reduction (MOR) approaches used in this work to generate reduced order models. Proper Orthogonal Decomposition (POD) is a dimension reduction procedure that generates optimal low order basis from ensembles of data, or *snapshots* of system trajectories. After that, Galerkin projection is utilized to produce reduced order models. The method of POD is reviewed and a splitting scheme for *snapshots* of nonlinear coupled systems (e.g. thermo-fluid system) is introduced. In reduced order modeling, it is of interest to preserve stability of the original full order model. The stabilization method for projection based reduced order models is described then. The POD method is efficient in constructing linear reduced order models. However, in the presence of a general nonlinearity, the computational complexity associated with evaluating high order nonlinear functions remains [27]. To overcome this issue, techniques for approximating nonlinear functions should be applied in conjunction with the POD method to further improve dimension reduction efficiency. A discrete empirical interpolation method (DEIM) is then described. The final POD-DEIM approach is applicable to construct nonlinear reduced order models.

### 2.2 Proper Orthogonal Decomposition

#### 2.2.1 Theory

Proper Orthogonal Decomposition (POD), also known as the Karhunen-Loève decomposition, principal component analysis (PCA) and several other names, is a popular method to derive reduced order models for dynamical systems [28, 29]. The POD approach has been applied in a wide range of disciplines, such as turbulent

flows [30], aerodynamics [31], and optimal control [32]. The fundamental idea of POD is that from a collection of samples under consideration, one can construct a low-dimension orthonormal basis that optimally represents the original data set. Snapshots of a dynamical system can either be numerical solutions or experimental observations. The nature of POD is similar to the Fourier modes: a function of interest is projected onto a set of basis functions or modes thus providing a finite set of scalar coefficients that represent the original function. The POD provides a particular set of modes that are linear basis for describing a finite set of observations, that minimizes the average squared distance between the original data set and its reduced linear representation. Consider a general dynamical system:

$$\dot{\mathbf{x}} = f(\mathbf{x}, \mathbf{u}) \quad (2.1)$$

where  $\mathbf{x} \in \mathbb{R}^N$  denotes the dynamic states,  $\mathbf{u} \in \mathbb{R}^m$  denotes the control inputs. POD is a technique for finding a basis which spans an ensemble of data collected from experiments or numerical simulations. Roughly speaking, it extracts a low-dimension basis from a large set of samples of the trajectories associated with different control inputs. Consider a set of trajectory snapshots:

$$\mathbf{X} = \begin{bmatrix} \mathbf{x}^{(1)} & \mathbf{x}^{(2)} & \dots & \mathbf{x}^{(p)} \end{bmatrix} \in \mathbb{R}^{N \times p}. \quad (2.2)$$

POD constructs an orthonormal basis that can represent principal characteristics of the snapshots matrix. Consider an orthonormal basis matrix:

$$\mathbf{V} = \begin{bmatrix} \mathbf{v}_1 & \mathbf{v}_2 & \dots & \mathbf{v}_k \end{bmatrix} \in \mathbb{R}^{N \times k} \quad (2.3)$$

The properties of orthogonality and unit vector length bring that,

$$\mathbf{v}_i^T \mathbf{v}_j = \begin{cases} 1 & i = j \\ 0 & i \neq j \end{cases} \quad (2.4)$$

which can be written in a compact way,

$$\mathbf{V}^T \mathbf{V} = \mathbf{I}_k \in \mathbb{R}^{k \times k} \quad (2.5)$$

where  $\mathbf{I}_k$  is the identity matrix.

As shown in Fig. 2.1, projection of the state vector  $\mathbf{x}$  onto an orthonormal basis  $\mathbf{V}$  results in an approximated state vector,

$$\hat{\mathbf{x}} = \mathbf{V}\mathbf{V}^T\mathbf{x} \quad (2.6)$$

Similarly, when each state vector of the snapshots matrix is projected onto the

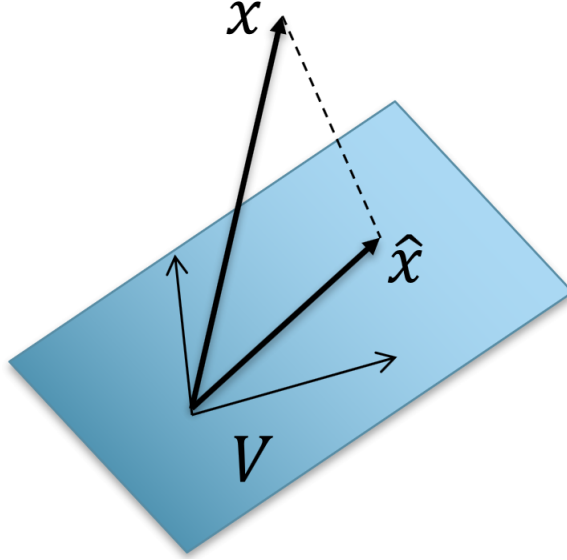


Fig. 2.1. Projection of states vector onto a basis.

basis, the approximation becomes  $\mathbf{x}^{(i)} \approx \mathbf{V}\mathbf{V}^T\mathbf{x}^{(i)}$ . POD constructs a basis which is optimal in the sense of approximation error, and the POD basis solves the following optimization problem:

$$\min \sum_{i=1}^p \|\mathbf{x}^{(i)} - \mathbf{V}\mathbf{V}^T\mathbf{x}^{(i)}\|^2 = \min \|\mathbf{X} - \mathbf{V}\mathbf{V}^T\mathbf{X}\|_F^2 \quad (2.7)$$

$$\text{s.t. } \mathbf{V}^T\mathbf{V} = \mathbf{I} \quad (2.8)$$

where  $\|\cdot\|_F$  denotes the Frobenius norm. Kunisch and Volkwein [32] demonstrated the close connection between POD and the Singular Value Decomposition (SVD) in constructing a reduced basis, and showed that the solution to the minimization

problem in (2.7) is a truncation of the left singular vector of the snapshot matrix  $\mathbf{X}$  with approximation error indicted by the singular values,

$$\sum_{i=1}^p \|\mathbf{x}^{(i)} - \mathbf{V}\mathbf{V}^T \mathbf{x}^{(i)}\|^2 = \sum_{j=k+1}^N \sigma_j^2 \quad (2.9)$$

where  $\sigma_j$  is the  $j^{\text{th}}$  singular value and the target basis  $\mathbf{V}$  is of dimension  $\mathbb{R}^{N \times k}$ . This facilitates solving the POD problem, since there are efficient and reliable tools to compute SVD of any rectangular matrix, for instance, the Matlab `svd()` function. However, memory could become an issue when the dimension of the snapshots matrix is extremely large. In reduced order modeling of a complex system, construction of reduced basis requires collecting a large number of trajectory samples to preserve dominant characteristics of the state space. This may result in a “fat” snapshot matrix  $\mathbf{X} \in \mathbb{R}^{N \times p}$  where  $p \gg N$ . Processing a large size matrix is not convenient due to large memory requirements. Thus, instead of directly computing SVD of the snapshot matrix,

$$\mathbf{X} = \mathbf{U}\mathbf{\Sigma}\mathbf{V}^T \quad (2.10)$$

one can compute SVD of  $\mathbf{X}\mathbf{X}^T$ , which can also be viewed as eigen-decomposition,

$$\mathbf{X}\mathbf{X}^T = \mathbf{U}\mathbf{\Sigma}\mathbf{\Sigma}^T\mathbf{U}^T \quad (2.11)$$

Note that the square matrix  $\mathbf{X}\mathbf{X}^T$  is of dimension  $N$ . Solving SVD of this matrix is much easier in terms of computing the left singular vectors.

Once the reduced order basis is generated, the corresponding POD reduced order models are constructed by applying Galerkin projection. The state space is first approximated by a linear combination of the reduced basis,

$$\mathbf{x}(t) \approx \sum_{i=1}^k a_i \mathbf{v}_i = \mathbf{V}\mathbf{a}(t) \quad (2.12)$$

where the coefficient vector  $\mathbf{a} \in \mathbb{R}^k$  will be the reduced states. Then projecting the governing equations of (2.1) onto the reduced basis results in the reduced system,

$$\dot{\mathbf{a}} = \mathbf{V}^T f(\mathbf{V}\mathbf{a}, \mathbf{u}) \quad (2.13)$$

### 2.2.2 Splitting State Space for Coupled Systems

In the field of engineering, systems of interests are often multivariable-coupled systems. It is challenging to construct a reduced order basis capable of capturing dominant characteristics for each state, since the magnitude and profile of different states may vary significantly. It can be seen from the derivation of POD in (2.7) that the reduced basis is optimal in terms of the average of all snapshots data but does not have physical meaning. Also, with the POD dimension reduction techniques, some states may be recognized as dominant features with a large weight for the approximation error, while other states can not be accurately approximated when we go back from the reduced space to the state space. Therefore, it is beneficial to split the snapshots and extract different reduced bases for different dynamic states. This approach is found to be efficient for multi-domain physical systems [33]. Furthermore, stabilization of a large-scale system can bring numerical challenges to the optimization algorithms, which will be discussed in the next section. The POD reduced order model under the splitting scheme is illustrated by a general dynamical system having two sets of states:

$$\begin{cases} \dot{\mathbf{x}}_1 = f_1(\mathbf{x}_1, \mathbf{x}_2) \\ \dot{\mathbf{x}}_2 = f_2(\mathbf{x}_1, \mathbf{x}_2) \end{cases} \quad (2.14)$$

where  $f_1, f_2$  are general nonlinear functions. The snapshot matrix is split into different sets representing different states, and POD bases are constructed from a set of snapshots corresponding to those states,

$$\begin{cases} \mathbf{x}_1 \approx \mathbf{V}_1 \mathbf{a}_1 \\ \mathbf{x}_2 \approx \mathbf{V}_2 \mathbf{a}_2 \end{cases} \quad (2.15)$$

where  $\mathbf{V}_1, \mathbf{V}_2$  are reduced bases extracted from the snapshots, and  $\mathbf{a}_1, \mathbf{a}_2$  are the corresponding reduced states. Projecting the original system onto the reduced bases gives the following reduced system,

$$\begin{cases} \dot{\mathbf{a}}_1 = \mathbf{V}_1^T f_1(\mathbf{V}_1 \mathbf{a}_1, \mathbf{V}_2 \mathbf{a}_2) \\ \dot{\mathbf{a}}_2 = \mathbf{V}_2^T f_2(\mathbf{V}_1 \mathbf{a}_1, \mathbf{V}_2 \mathbf{a}_2). \end{cases} \quad (2.16)$$

Note that the resulting reduced system is still coupled, but the accuracy can be better preserved when approximating the state space.

### 2.3 Stabilization of POD Reduced Order Models

When considering model order reduction, it is essential to preserve the stability property from the original high-fidelity model without significantly affecting the accuracy, because projection-based model reduction methods, such as POD, often result in a reduced order model without stability guarantee. Consider a linear time-invariant (LTI) system,

$$\dot{\mathbf{x}} = A\mathbf{x} \quad (2.17)$$

where  $\mathbf{x} \in \mathbb{R}^N, A \in \mathbb{R}^{N \times N}$ . The system is said to be asymptotically stable if the Lyapunov equation

$$PA + A^H P \prec \mathbf{0} \quad (2.18)$$

has a symmetric positive definite solution  $P$ . A reduced order system directly obtained from the POD basis  $V \in \mathbb{R}^{k \times k}$  is of the form

$$\dot{\mathbf{a}} = V^T A V \mathbf{a} = \tilde{A} \mathbf{a} \quad (2.19)$$

where  $\tilde{A} \in \mathbb{R}^{k \times k}$  represents the reduced dynamics. (2.19) actually shows that stability of the reduced order model is system and basis variant. For the same system, the choice of reduced order basis (ROB) can definitely lead to reduced order models with different properties. However, Prajna [34] showed that certain properties of the original system can guarantee preservation of stability for reduced order models

regardless of choice of the basis functions. Assume the original system in (2.17) is asymptotically stable (all eigenvalues have negative real part). The POD model reduction is guaranteed to preserve stability irrespective of the basis used, if the Hermitian part of matrix  $A$  is negative definite

$$A + A^H \prec \mathbf{0}. \quad (2.20)$$

Suppose the system in (2.17) meets this condition, then for an arbitrary POD basis  $\mathbf{V} \in \mathbb{R}^{N \times k}$ , we have

$$\mathbf{V}^T(A + A^H)\mathbf{V} \prec \mathbf{0} \quad (2.21)$$

since the POD basis has full column rank. It follows that

$$\mathbf{V}^T A \mathbf{V} + (\mathbf{V}^T A \mathbf{V})^H \prec \mathbf{0} \quad (2.22)$$

since  $\mathbf{V}$  is a real matrix so that  $\mathbf{V}^T = \mathbf{V}^H$ . Note that  $\mathbf{V}^T A \mathbf{V}$  is the reduced dynamics in (2.19), which can be written as

$$\tilde{A} + \tilde{A}^H \prec \mathbf{0} \quad (2.23)$$

The next step is to prove that the condition of (2.23) will result in matrix  $\tilde{A}$  having eigenvalues with negative real part. Let  $\lambda$  be any eigenvalue of  $\tilde{A}$ , and  $\mathbf{v}$  be the corresponding eigenvector,

$$\tilde{A}\mathbf{v} = \lambda\mathbf{v}. \quad (2.24)$$

A quadratic form of (2.23) is

$$\mathbf{v}^H(\tilde{A} + \tilde{A}^H)\mathbf{v} < 0. \quad (2.25)$$

It follows that

$$\begin{aligned} & \mathbf{v}^H \lambda \mathbf{v} + (\lambda \mathbf{v})^H \mathbf{v} \\ &= (\lambda + \lambda^*) \mathbf{v}^H \mathbf{v} \\ &= (\lambda + \lambda^*) \|\mathbf{v}\|^2 \end{aligned} \quad (2.26)$$

where  $\lambda^*$  is the complex conjugate. Since  $\|\mathbf{v}\|^2 > 0$ , then the real part of  $\lambda$  is negative, and the reduced order model is asymptotically stable. This sufficient condition of

stability guarantee can be used as a *prior* knowledge in model reduction. When it is not the case for some systems to automatically preserve the stability, Prajna [34] proposed a stabilization scheme through a state transformation.

From the Lyapunov equation in (2.18), let  $P^{\frac{1}{2}}$  be the positive definite matrix such that  $P^{\frac{1}{2}}P^{\frac{1}{2}} = P$ . Defining the transformed states

$$\mathbf{y} = P^{\frac{1}{2}}\mathbf{x} \quad (2.27)$$

and substituting into (2.17) results in the transformed system

$$\dot{\mathbf{y}} = P^{\frac{1}{2}}AP^{-\frac{1}{2}}\mathbf{y} \quad (2.28)$$

By checking the Hermitian part, it follows that

$$\begin{aligned} & P^{\frac{1}{2}}AP^{-\frac{1}{2}} + (P^{\frac{1}{2}}AP^{-\frac{1}{2}})^H \\ &= P^{-\frac{1}{2}}(PA + A^HP)P^{-\frac{1}{2}} \prec \mathbf{0} \end{aligned} \quad (2.29)$$

which indicates that the transformed system satisfies the condition of (2.20), and thus the POD reduced order model will preserve the stability for any basis generated from the transformed states. Note that solution to the Lyapunov equation (2.18) is not unique. In practice, the symmetric positive definite matrix  $P$  is usually solved by specifying a negative definite matrix  $Q$

$$PA + A^HP = Q. \quad (2.30)$$

Therefore, the degree of freedom in choosing  $Q$  can be utilized to form an optimization problem for some certain objectives. For example, it is beneficial to minimize the modification to eigenvalues of the original model. If in some directions, the eigenvalues are scaled to be too large, simulation of the transformed system may experience numerical failure, because the integration time step should be small enough to meet the error tolerance. On the other hand, a very small scaling factor is also problematic, since numerically the stability of such a system is not guaranteed if the poles are too close to zero. In other words, the system will be sensitive to estimation error of the states if the dynamics matrix in (2.28) is ill-conditioned. For the reasons given above,

it is desirable to keep the condition number (the ratio of the largest eigenvalue to the smallest eigenvalue, which is always greater than or equal to one by definition) of  $P$  as close as possible to one. The optimization problem [34] is stated below:

$$\begin{cases} \min & \gamma \\ \text{s.t.} & PA + A^H P \prec \mathbf{0} \\ & I - P \prec \mathbf{0} \\ & P - \gamma I \prec \mathbf{0} \end{cases} \quad (2.31)$$

wherein,  $\gamma$  is condition number, and  $I$  is the identity matrix.

For reduced order modeling of nonlinear systems, one can linearize at an equilibrium point and apply the above scheme to get a locally stabilized reduced model. However, when it is desired to ensure stability at various equilibrium points for complex nonlinear systems, this approach is not applicable because it is unable to obtain a global set of transformed states.

Instead of directly operating on the original full order model before projection onto a reduced basis, Amsallem and Farhat [35] proposed a stabilization scheme that operates on readily generated ROB by POD. The method is motivated by semidefinite programming [36], and requires primarily the solution of a convex optimization problem. It fixes one of the ROB, for instance, the right one, and modifies the other one to enforce the stability of the resulting projection-based reduced order model. Consider the LTI system in (2.17), The state space is first approximated by a linear combination of columns of a reduced basis  $V_k \in \mathbb{R}^{N \times k}$  as shown in (2.12). Then search for another reduced basis  $W_k \in \mathbb{R}^{N \times k}$  and project the system onto it, such that the resulting reduced order model is asymptotically stable,

$$W_k^T V_k \dot{\mathbf{a}} = W_k^T A V_k \mathbf{a} \quad \mathbf{a} \in \mathbb{R}^k \quad (2.32)$$

where  $W_k$  is usually denoted as the left ROB, and  $V_k$  as the right ROB. As mentioned before, the system is asymptotically stable if the Lyapunov equation has a symmetric

positive definite solution. Since (2.32) is posed in descriptor form, the generalized Lyapunov equation for the system  $E\dot{\mathbf{x}} = A\mathbf{x}$  is formed as

$$E^T P A + A^T P E \prec \mathbf{0}. \quad (2.33)$$

In this case,  $E = W_k^T V_k$  and  $A = W_k^T A V_k$ . Substituting into (2.33), one can write,

$$V_k^T W_k P W_k^T A V_k + V_k^T A^T W_k P W_k^T V_k \prec \mathbf{0} \quad (2.34)$$

The main idea of the stabilization method is to minimally modify the left ROB  $W_k$ , such that system (2.32) is asymptotically stable. In the POD method, a general ROB  $V \in \mathbb{R}^{N \times N}$  without truncation is already constructed, which is optimal to represent the empirical data. Hence the stabilization method can start from the range of  $V$ . Consider a ROB  $W_{k+p} \in \mathbb{R}^{N \times (k+p)}$  ( $k+p < N$ ) which is a truncation of POD basis  $V$ . Then search for a left ROB  $W_k$  of dimension  $k$  (the target dimension of the reduced order model), in the subspace range  $W_{k+p}$ , while meeting the stability requirement in (2.33). Because  $W_k$  is in the range of  $W_{k+p}$ , it can be written as

$$W_k = W_{k+p} Z \quad (2.35)$$

where  $Z \in \mathbb{R}^{(k+p) \times k}$ . Replacing  $W_k$  with it in (2.34), the Lyapunov equation can be written in variable  $Z$ ,

$$V_k^T W_{k+p} Z P Z^T W_{k+p}^T A V_k + V_k^T A^T W_{k+p} Z P Z^T W_{k+p}^T V_k \prec \mathbf{0} \quad (2.36)$$

which will be used as constraints to form an optimization problem. In terms of the objective function, a possible choice can be minimizing the modification of POD basis to obtain  $W_k$ ,

$$f(Z) = \|W_{k+p} Z - V_k\| \quad (2.37)$$

where  $\|\cdot\|$  denotes any matrix norm. This minimization meets the requirement for a stabilization scheme to preserve the accuracy as much as possible. Note that if

$$Z = \begin{bmatrix} \mathbf{e}_1, \mathbf{e}_2, \dots, \mathbf{e}_k \end{bmatrix} \quad (2.38)$$

where  $\mathbf{e}_i$  is the  $i^{\text{th}}$  column of the identity matrix  $I \in \mathbb{R}^{(k+p) \times (k+p)}$ . Then this is just extracting the first  $k$  columns from matrix  $W_{k+p}$ , which is  $V_k$ . Furthermore, the resulting reduced model is exactly the same as (2.19), which means no stabilization effort is needed for the conventional POD reduced model.

Finally the following minimization problem is formed:

$$\min \|W_{k+p}Z - V_k\| \quad (2.39)$$

$$\text{s.t. } V_k^T W_{k+p} Z P Z^T W_{k+p}^T A V_k + V_k^T A^T W_{k+p} Z P Z^T W_{k+p}^T V_k \prec \mathbf{0} \quad (2.40)$$

Note that the constraint in this problem is not convex in the variable  $Z$  because of the term  $Z P Z^T$ . In order to apply techniques from convex optimization, the change of variable

$$\tilde{P} = Z P Z^T \quad (2.41)$$

is introduced. Correspondingly, the objective should be modified and expressed in  $\tilde{P}$ . It is proved in [35] that if there exists an symmetric positive semidefinite matrix  $\hat{P}$ , which can be partitioned in blocks as

$$\hat{P} = \begin{bmatrix} \hat{P}_{11} & \hat{P}_{12} \\ \hat{P}_{12}^T & \hat{P}_{22} \end{bmatrix} \quad (2.42)$$

where  $\hat{P}_{11} \in \mathbb{R}^{k \times k}$  then the solution of the minimization problem (2.39) can be constructed as

$$\tilde{P} = \begin{bmatrix} \hat{P}_{11} \\ \hat{P}_{12}^T \end{bmatrix} \hat{P}_{11}^{-1} \begin{bmatrix} \hat{P}_{11} & \hat{P}_{12} \end{bmatrix}. \quad (2.43)$$

Then it follows that

$$Z = \begin{bmatrix} \hat{P}_{11} \\ \hat{P}_{12}^T \end{bmatrix} \quad (2.44)$$

In practice, the optimization problem of interest can be directly solved using convex optimization packages, such as CVX [37].

Now consider the system under the states splitting scheme in (2.14). Since groups of states are approximated by different POD bases, the stabilization method cannot be directly used for the overall system. Instead, one can fix one of the POD bases,

and modify the others by the semidefinite programming method mentioned above, to stabilize the coupled system. Suppose that the reduced order model of system (2.14) is stabilized at some equilibrium points. Linearizing the system at one of the equilibrium points  $\mathbf{x}_0$  gives the following system,

$$\begin{bmatrix} \dot{\mathbf{x}}_1 \\ \dot{\mathbf{x}}_2 \end{bmatrix} = \begin{bmatrix} A_{11} & A_{12} \\ A_{21} & A_{22} \end{bmatrix} \left( \begin{bmatrix} \mathbf{x}_1 \\ \mathbf{x}_2 \end{bmatrix} - \begin{bmatrix} \mathbf{x}_{01} \\ \mathbf{x}_{02} \end{bmatrix} \right) \quad (2.45)$$

where  $A_{ij}$  is the corresponding Jacobian matrix. By replacing the original states with reduced order states and projecting the system onto reduced bases, the coupled reduced system is of the form

$$\begin{bmatrix} \dot{\mathbf{a}}_1 \\ \dot{\mathbf{a}}_2 \end{bmatrix} = \begin{bmatrix} V_1^T & \mathbf{0} \\ \mathbf{0} & V_2^T \end{bmatrix} \begin{bmatrix} A_{11} & A_{12} \\ A_{21} & A_{22} \end{bmatrix} \begin{bmatrix} V_1 & \mathbf{0} \\ \mathbf{0} & V_2 \end{bmatrix} \left( \begin{bmatrix} \mathbf{a}_1 \\ \mathbf{a}_2 \end{bmatrix} - \begin{bmatrix} \mathbf{a}_{01} \\ \mathbf{a}_{02} \end{bmatrix} \right). \quad (2.46)$$

If the system after projection is unstable, one set of equations should instead be projected onto a particularly constructed basis from the stabilization scheme. For example, equations associated with states  $\mathbf{x}_1$  are still projected onto  $V_1$  and those associated with  $\mathbf{x}_2$  will be projected onto a new basis  $W_2$ , which makes the reduced system stable,

$$\begin{bmatrix} I & \mathbf{0} \\ \mathbf{0} & W_2^T V_2 \end{bmatrix} \begin{bmatrix} \dot{\mathbf{a}}_1 \\ \dot{\mathbf{a}}_2 \end{bmatrix} = \begin{bmatrix} V_1^T & \mathbf{0} \\ \mathbf{0} & W_2^T \end{bmatrix} \begin{bmatrix} A_{11} & A_{12} \\ A_{21} & A_{22} \end{bmatrix} \begin{bmatrix} V_1 & \mathbf{0} \\ \mathbf{0} & V_2 \end{bmatrix} \left( \begin{bmatrix} \mathbf{a}_1 \\ \mathbf{a}_2 \end{bmatrix} - \begin{bmatrix} \mathbf{a}_{01} \\ \mathbf{a}_{02} \end{bmatrix} \right). \quad (2.47)$$

Since it is a coupled dynamical system, applying the Lyapunov equation will bring additional terms such as the product  $W_{k+p}XP$  in the cross term of different states, which makes the problem nonconvex in the variables  $X$  and  $P$ . It is very challenging to stabilize the coupled system, but one possible attempt is to replace the term  $W_{k+p}X$  with the constant matrix  $V_k$ , which is the solution in the ideal case.

## 2.4 Discrete Empirical Interpolation Method

The standard POD model reduction technique reduces dimension of states, and was shown to be computationally efficient for LTI systems [29,38]. However, there is

an issue associated with nonlinear model reduction problems. Consider a system of general nonlinear ODEs,

$$\dot{\mathbf{x}} = A\mathbf{x} + f(\mathbf{x}, \mathbf{u}) \quad (2.48)$$

where  $\mathbf{x} \in \mathbb{R}^N$  denotes the state vector, whose dimension  $N$  is typically large in high-fidelity models arising from finite difference or finite volume discretization,  $A$  is a constant coefficient matrix representing the linear part of this system,  $f$  represents the nonlinear functions, and  $\mathbf{u} \in \mathbb{R}^d$  denotes the control inputs. Projection-based model order reduction methods including POD seek a reduced order basis whose linear combinations can approximate the input-output responses of the original high-dimension system, and is optimal in the sense of a certain approximation error. By replacing the states  $\mathbf{x}$  with  $V\mathbf{a}$ , and projecting the system in (2.48) onto the reduced basis  $V$ , the reduced order system is of the form

$$\dot{\mathbf{a}} = \tilde{A}\mathbf{a} + V^T f(V\mathbf{a}, \mathbf{u}) \quad (2.49)$$

where  $\mathbf{a} \in \mathbb{R}^k, k \ll N$  denotes the reduced states and  $\tilde{A} = V^T A V \in \mathbb{R}^{k \times k}$  represents the reduced order linear functions. It can be observed from (2.49) that though the number of states and linear equations are reduced, the computational complexity of evaluating the high-order nonlinear term  $f$  remains. To overcome this issue, techniques for approximating nonlinear functions should be used in conjunction with the POD model reduction method to further improve dimension reduction efficiency. A discrete empirical interpolation method (DEIM) was successfully used to improve the computational efficiency of projection-based nonlinear reduced order models [27]. It constructs specially selected interpolation indices to minimize a certain upper bound of the approximation error. It is applicable to ODEs arising from finite difference or finite volume discretization of time dependent PDEs or parametrically dependent steady state problems. The DEIM approach can be viewed as a combination of projection and interpolation. It performs an interpolation-based projection to provide an optimal subspace approximation to the nonlinear term without the expense of orthogonal projection.

An effective way to overcome the issue described above is to approximate the nonlinear term in (2.49) by projecting it onto a reduced basis of dimension  $m \ll N$ , that approximates the nonlinear function space. Recall that a POD reduced order model is generated from *snapshots* of system trajectories. Here the same procedure is adopted to extract a subspace spanned by the basis  $U \in \mathbb{R}^{N \times m}$  from a collection of nonlinear dynamics:

$$F = [\mathbf{f}^{(1)}, \mathbf{f}^{(2)}, \dots, \mathbf{f}^{(q)}] \in \mathbb{R}^{N \times q}. \quad (2.50)$$

It should be noted that nonlinear functions need to be evaluated to generate system trajectories (2.2) in the standard POD procedure, and hence no additional computational cost is added to the original model reduction problem. However, more computer memory is required to store the values of nonlinear functions, which can be problematic when the number of snapshot samples is significantly large. The nonlinear functions are approximated by projection onto a reduced basis,

$$\mathbf{f}(t) \approx U\mathbf{c}(t) \quad (2.51)$$

where  $U \in \mathbb{R}^{N \times m}$  is obtained by applying POD to the nonlinear snapshots matrix  $F$  in (2.50), and  $\mathbf{c}$  is a vector of the corresponding time coefficients. To calculate the coefficients from the overdetermined system in (2.51),  $m$  distinguished rows are selected to form a well-posed system. Consider an interpolation scheme

$$P^T \mathbf{f}(t) \approx P^T U \mathbf{c}(t) \quad (2.52)$$

where  $P \in \mathbb{R}^{N \times m}$  is a matrix whose  $i^{\text{th}}$  column  $\mathbf{e}_{\zeta_i} = [0, \dots, 0, 1, 0, \dots, 0]^T$  is the  $\zeta_i^{\text{th}}$  column of the identity matrix  $I \in \mathbb{R}^{N \times N}$ ,

$$P = [\mathbf{e}_{\zeta_1}, \mathbf{e}_{\zeta_2}, \dots, \mathbf{e}_{\zeta_m}]. \quad (2.53)$$

Suppose that  $P^T U$  is non-singular, then the coefficients can be uniquely determined and the final interpolation approximation of the nonlinear functions is

$$\tilde{\mathbf{f}}(t) = U(P^T U)^{-1} P^T \mathbf{f}(t). \quad (2.54)$$

It can be shown that  $\tilde{\mathbf{f}}(t)$  is indeed an interpolation approximation of the original function  $\mathbf{f}$ . Applying the interpolation one more time yields that  $\tilde{\mathbf{f}}$  is exact at the chosen interpolation indices.

$$P^T \tilde{\mathbf{f}} = P^T U (P^T U)^{-1} P^T \mathbf{f}(t) = P^T \mathbf{f}(t). \quad (2.55)$$

Note that  $P$  and  $U$  are constant matrices, so the matrix multiplication can be precomputed before the online simulation.  $P^T \mathbf{f}(t)$  can be seen as evaluating some of the functions from the original high order system at the specified interpolation indices, which will significantly reduce the computational load. To complete the DEIM, Chaturantabut and Sorensen [27] proposed an algorithm for determining interpolation indices inductively from the basis  $U$ . The interpolation points are selected to limit growth of an error bound, and are guaranteed to be hierarchical and non-repeated. The algorithm is shown by the following pseudocode:

```

Input: a POD basis  $\begin{bmatrix} \mathbf{u}_1 & \dots & \mathbf{u}_m \end{bmatrix}$ 
Output: Indices  $\boldsymbol{\zeta} = \begin{bmatrix} \zeta_1 & \zeta_2 & \dots & \zeta_m \end{bmatrix}^T \in \mathbb{R}^m$ 
1 :  $\left[ |\theta|, \zeta_1 \right] = \max(|\mathbf{u}_1|)$ 
2 :  $\mathbf{U} = \begin{bmatrix} \mathbf{u}_1 \end{bmatrix}, P = \begin{bmatrix} \mathbf{e}_{\zeta_1} \end{bmatrix}, \boldsymbol{\zeta} = \begin{bmatrix} \zeta_1 \end{bmatrix}$ 
3 : for  $l = 2$  to  $m$  do
4 :   Solve  $(\mathbf{P}^T \mathbf{U}) \mathbf{c} = \mathbf{P}^T \mathbf{u}_l$  for  $\mathbf{c}$ 
5 :    $\mathbf{r} = \mathbf{u}_l - \mathbf{U} \mathbf{c}$ 
6 :    $\left[ |\theta|, \zeta_l \right] = \max(|\mathbf{r}|)$ 
7 :    $\mathbf{U} \leftarrow \begin{bmatrix} \mathbf{U} & \mathbf{u}_l \end{bmatrix}, \mathbf{P} \leftarrow \begin{bmatrix} \mathbf{P} & \mathbf{e}_{\zeta_l} \end{bmatrix}, \boldsymbol{\zeta} \leftarrow \begin{bmatrix} \boldsymbol{\zeta}^T & \zeta_l \end{bmatrix}$ 
8 : end for.
```

The notation  $\max$  in steps 1 and 6 are the same as the **max** function in MATLAB, which returns the maximum elements of an array and its index. Chaturantabut

and Sorensen [27] proved that an approximated error bound of the DEIM algorithm described above can be obtained by

$$\|\mathbf{f} - \tilde{\mathbf{f}}\|_2 \approx \|(P^T U)^{-1}\|_2 \sigma_{m+1} \quad (2.56)$$

where  $\sigma_{m+1}$  is the  $(m+1)^{th}$  leading singular value of the nonlinear function *snapshots* matrix in (2.50). In practice, it can be used in determining the number of interpolation points. As more functions are evaluated, the approximation error is smaller since the singular values are arranged in descending order from SVD. When there's a significant gap between the magnitude of two adjacent singular values, the number of indices  $m$  could be determined at that point.

## 3. REDUCED ORDER MODELING FOR VCC

### 3.1 Introduction

This chapter presents a nonlinear model order reduction framework for vapor compression cycles. The finite volume heat exchanger model is reformulated by choosing a different pair of thermodynamic states, to enable application of nonlinear model reduction techniques. Then a staggered grid is implemented for discretization. The POD in conjunction with the DEIM approach are used to generate reduced order heat exchanger models. After that, a fast thermodynamic properties evaluation scheme based on Artificial Neural Networks is described. The reduced order heat exchanger models coupled with quasi-static models of the compressor and expansion valve are implemented in Modelica-based simulation tools. Finally numerical treatments are introduced to improve model robustness.

### 3.2 Reformulation of Finite Volume Model

#### 3.2.1 Governing Equations

To enable the use of nonlinear model order reduction (NL-MOR) techniques on a dynamic heat exchanger (HX) model, the typical finite volume (FV) model [5], which applies refrigerant pressure and enthalpies as dynamic states, needs to be converted to the standard form of NL-MOR. This is because the FV formulation consisting of refrigerant pressure, enthalpies as states as well as an elimination process of interface

mass flow rates, has a descriptor form. It can be seen from the discretized governing equations of the  $j^{\text{th}}$  control volume for refrigerant flow:

$$\left(\frac{\partial \rho_j}{\partial P}\right)_{h_j} \frac{dP}{dt} + \left(\frac{\partial \rho_j}{\partial h}\right)_P \frac{dh_j}{dt} = \frac{1}{V_j}(\dot{m}_{j-1} - \dot{m}_j) \quad (3.1)$$

$$\left(h_j \frac{\partial \rho_j}{\partial P} - 1\right)_{h_j} \frac{dP}{dt} + \left(h_j \frac{\partial \rho_j}{\partial h} + \rho_j\right)_P \frac{dh_j}{dh} = \frac{1}{V_j}(\dot{m}_{j-1}h_{j-1} - \dot{m}_jh_j - \dot{Q}_j). \quad (3.2)$$

Due to the partial derivatives of refrigerant density with respect to pressure and enthalpy in the mass balance and energy balance, the system of interest is in a descriptor form

$$E(\mathbf{x})\dot{\mathbf{x}} = F(\mathbf{x}, \mathbf{u}) \quad (3.3)$$

where  $\mathbf{x}$  is the state vector consisting of refrigerant pressure, enthalpies, tube and secondary fluid temperatures.  $\mathbf{u}$  denotes boundary conditions including refrigerant inlet and outlet mass flow rates, inlet enthalpy, the secondary fluid inlet mass flow rate and temperature.

$$\mathbf{x} = \left[ P, h_1, \dots, h_N, T_{t1}, \dots, T_{tN}, T_{w1}, \dots, T_{wN} \right]^T \quad (3.4)$$

$$\mathbf{u} = \left[ \dot{m}_i, \dot{m}_{out}, h_i, T_{w,i}, \dot{m}_{w,i} \right]^T. \quad (3.5)$$

However, implementing NL-MOR requires the dynamical system of the standard ordinary differential equation (ODE) form in (2.1). It is clear that the mismatched model structure of the FV-HX with respect to the baseline NL-MOR cannot be directly used for the purpose. A reformulated FV-HX model using a different pair of thermodynamic states with appropriate assumptions should be derived to match the standard ODE structure. A HX model selecting refrigerant density, internal energy and interface mass flow rates as dynamic states was developed. Correspondingly, the momentum balance is integrated into governing equations to evaluate dynamics of the interface mass flow rates. First, the following assumptions are made for deriving the set of governing equations to describe flow phenomena within heat exchangers.

- one-dimensional flow of refrigerant and the secondary fluid;

- changes in kinetic energy and potential energy are negligible;
- viscous dissipation is negligible;
- axis heat conduction is dropped from consideration.

With these assumptions, the governing equations of refrigerant mass, momentum and energy balances can be written as follows [39]:

$$\frac{\partial}{\partial t}(\rho A_c) + \frac{\partial}{\partial z}(\rho A_c v) = 0 \quad (3.6)$$

$$\frac{\partial}{\partial t}(\rho A_c v) + \frac{\partial}{\partial z}(\rho A_c v^2) + A_c \frac{\partial P}{\partial z} + \frac{A_r}{L} \tau = 0 \quad (3.7)$$

$$\frac{\partial}{\partial t}(\rho A_c u) + \frac{\partial}{\partial z}(\rho A_c v h) + \frac{\alpha A_r}{L} (T_r - T_t) = 0 \quad (3.8)$$

where  $\rho$  is refrigerant density,  $A_c$  is the cross flow area,  $z$  is the refrigerant flow axis,  $v$  is velocity,  $P$  is pressure,  $u$  is internal energy,  $h$  is enthalpy,  $T_r$  is refrigerant temperature,  $T_t$  is tube temperature,  $A_r$  is heat transfer area,  $\alpha$  is the heat transfer coefficient. All properties represent the averages at position  $z$ . The counter-flow arrangement assumption is selected for heat exchanger models development in this work. Also, only the single-phase liquid, such as water or water&glycol mixture is employed as the secondary fluid. As a result, a tube material energy balance, and a secondary fluid energy balance can be derived:

$$(C_{pt}\rho_t A_t) \frac{\partial T_t}{\partial t} = \frac{\alpha_r A_r}{L} (T_r - T_t) - \frac{\alpha_w A_w}{L} (T_t - T_w) \quad (3.9)$$

$$(C_{pw}\rho_w A_w) \frac{\partial T_w}{\partial t} = (C_{pw}\rho_w A_w v_w) \frac{\partial T_w}{\partial z} - \frac{\alpha_w A_w}{L} (T_t - T_w) \quad (3.10)$$

The partial differential equations (PDEs) can be solved by discretizing spatially and then integrating in time domain. Finite volume method is chosen here and a set of ODEs is derived in the next section.

### 3.2.2 Discretization

In the finite volume model, the domain of the refrigerant flow is discretized into  $N$  control volumes. Integrating the governing equations over the length of each volume yields a system of ODEs as:

$$\frac{d\rho_j}{dt} = \frac{1}{V_j}(\dot{m}_k - \dot{m}_{k+1}) \quad (3.11)$$

$$\frac{d\dot{m}_k}{dt} = \frac{1}{L} \left( \dot{m}_{j-1}v_{j-1} - \dot{m}_jv_j + A_c(P_{j-1} - P_j) - F_f \right) \quad (3.12)$$

$$\frac{du_j}{dt} = \frac{1}{V_j\rho_j} \left( \dot{m}_kh_{j-1} - \dot{m}_{k+1}h_j - \dot{Q}_{r,j} + u_j(\dot{m}_{k+1} - \dot{m}_k) \right) \quad (3.13)$$

$$\frac{dT_{t,j}}{dt} = \frac{\dot{Q}_{r,j} - \dot{Q}_{w,j}}{M_{t,j}C_{pt}} \quad (3.14)$$

$$\frac{dT_{w,j}}{dt} = \frac{\dot{m}_wC_{pw}(T_{w,j+1} - T_{w,j}) + \dot{Q}_{w,j}}{M_{w,j}C_{pw}} \quad (3.15)$$

Note that a staggered grid scheme is utilized to derive the above equations. This scheme is commonly used in computational fluid dynamics to decouple the mass and energy balances from the momentum balance. It is claimed to give better convergence properties to avoid non-physical pressure variations [40–42]. As shown in Fig. 3.1, equations for refrigerant mass and energy balances (indices  $j$ ) are solved in the volume cells (black solid line), and momentum balances (indices  $k$ ) are solved in the flow cells (red dash line).

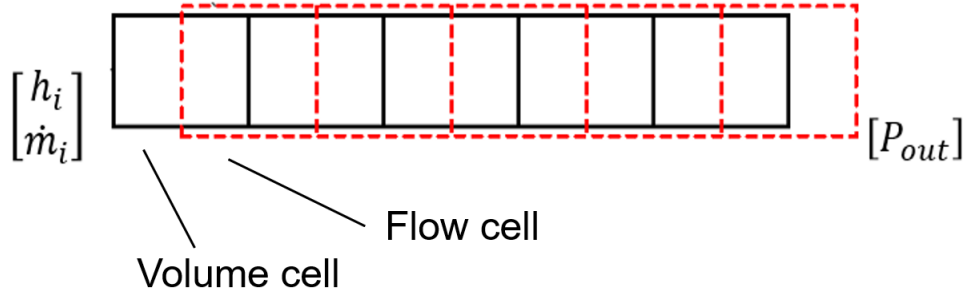


Fig. 3.1. Staggered grid for discretization on the refrigerant side

Pressures and enthalpies are calculated as functions of density and internal energy of each volume  $P_j(\rho_j, u_j), h_j(\rho_j, u_j)$ . The momentum at the interface of flow cell is evaluated by the average mass flow rates of flow cells

$$\dot{I}_j = \dot{m}_j v_j = \frac{\dot{m}_j^2}{\rho_j A_c} = \frac{(\dot{m}_{k-1} + \dot{m}_k)^2}{4\rho_j A_c} \quad (3.16)$$

where  $A_c$  is the cross flow area. The friction loss term [24] in the momentum balance is evaluated by

$$F_f = \mu A_c \frac{\dot{m}_k^2}{\bar{\rho}_k} \quad (3.17)$$

where  $\bar{\rho}_k$  is the average density of the flow cell  $k$ , and  $\mu$  is the frictional factor.

Correspondingly, boundary conditions consist of refrigerant mass flow rate and enthalpy at the heat exchanger inlet, and refrigerant pressure at outlet. For the secondary fluid (e.g. water) side, boundary conditions are inlet mass flow rate and temperature. In addition, it is noted that the HX model under this scheme always

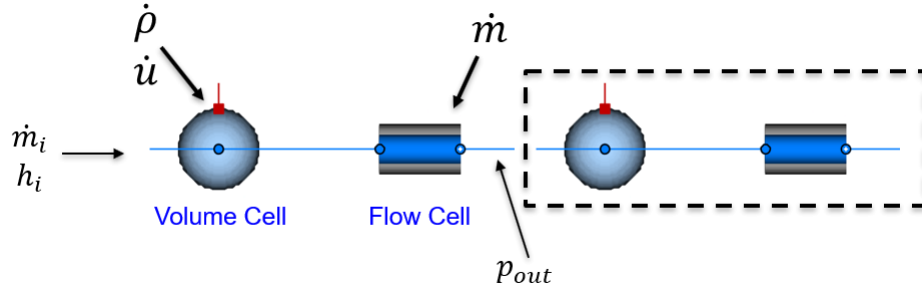


Fig. 3.2. Control volume object of the reformulated HX model.

starts at a volume cell, and ends at a flow cell. A volume cell followed by a flow cell can be regarded as an independent control volume, and treated as an object when implemented in object-oriented modeling languages, e.g. Modelica. As shown in Fig. 3.2, the control volume starts with a volume cell, where the dynamics of refrigerant density and internal energy are evaluated. The boundary conditions are the mass flow rate and enthalpy of the previous control volume. It is followed by a flow cell where the momentum balance is evaluated, and the boundary condition is the refrigerant pressure from the next control volume. Then users can simply declare a number of

control volumes based on the discretization level, and connect them to produce a HX model. This is also the way some popular Modelica libraries are developed, e.g. ThermoFluid [40], TIL [43]. The final HX model is in the standard ODE structure as desired with states and boundary conditions:

$$\mathbf{x} = \left[ \rho_1, \dots, \rho_N, \dot{m}_1, \dots, \dot{m}_N, u_1, \dots, u_N, T_{t1}, \dots, T_{tN}, T_{w1}, \dots, T_{wN} \right]^T \quad (3.18)$$

$$\mathbf{u} = \left[ \dot{m}_i, h_i, P_e, T_{w,i}, \dot{m}_{w,i} \right]^T \quad (3.19)$$

Furthermore, a staggered grid is necessary for the purpose of model order reduction. Note that the stabilization methods for reduced order models are based on semidefinite programming, which requires solving the Lyapunov equation. The Lyapunov stability criterion for LTI systems has a unique solution if and only if the system is asymptotically stable, which is equivalent to having all eigenvalues with strictly negative real part. For finite volume heat exchanger models, it is also possible to apply a staggered grid with  $N$  volume cells and  $N - 1$  flow cells to evaluate the dynamics of  $N - 1$  interface refrigerant mass flow rates [42]. In that way the boundary conditions are applied to the volume cells, and will be the same as the standard FV model. Though the system is solvable, the problem is that governing equations are not independent, which will result in a marginally stable system with non-positive eigenvalues, but not strictly negative. Therefore, the discretization scheme in Fig. 3.1 should be used for the purpose of this work. It can be verified that under this scheme, the HX model has strictly negative poles.

### 3.3 POD-DEIM Heat Exchanger Models

A nonlinear model order reduced framework based on the Proper Orthogonal Decomposition and the Discrete Empirical Interpolation Method was developed to generate reduced order heat exchanger models. The execution of the full order reformulated FV model produces snapshots of system trajectories as well as nonlinear functions. The empirical snapshots data is split based on dynamic states originating from the finite volume discretization. For example, a density snapshot matrix

is the collection of density trajectories of all control volumes. Since tube material and the secondary fluid (e.g. water) temperatures have very similar dynamics and magnitudes, their snapshots are grouped together, and only one reduced basis will be constructed for these states. Eventually, four groups of bases are generated to approximate system states respectively,

$$\boldsymbol{\rho} \approx V_\rho \mathbf{a}_\rho \quad (3.20)$$

$$\mathbf{u} \approx V_u \mathbf{a}_u \quad (3.21)$$

$$\dot{\mathbf{m}} \approx V_m \mathbf{a}_m \quad (3.22)$$

$$\mathbf{T} \approx V_T \mathbf{a}_T. \quad (3.23)$$

The reduced order basis for each group of states is extracted from the snapshots by the POD algorithm in (2.7). Using SVD to decompose the snapshot matrix, one can obtain an orthonormal basis from the left singular vectors. For example, the temperature snapshots including  $p$  trajectory samples,

$$\tilde{\mathbf{T}} = \left[ \mathbf{T}^{(1)} \quad \mathbf{T}^{(2)} \quad \dots \quad \mathbf{T}^{(p)} \right] \in \mathbb{R}^{N \times p} \quad (3.24)$$

where  $N$  is the number of states ( $N \ll p$ ), then  $\tilde{\mathbf{T}}$  can be decomposed into

$$\tilde{\mathbf{T}} = U \Sigma V^T. \quad (3.25)$$

The POD basis is a truncation of the left singular vectors  $U \in \mathbb{R}^{N \times N}$ . It is constructed by selecting  $k$  columns of  $U$ , corresponding to the first  $k$  dominant singular values ( $k < N$ ). The choice of the reduced basis dimension  $k$  is certainly of central importance for applying POD, as a tradeoff between approximation accuracy and computational savings. Observing the magnitude of singular values can be a natural criterion, since (2.9) shows that POD approximation error is connected with singular values. In practice, the ratio of the amount of energy captured by the POD basis to the total energy is usually used to determine the dimension,

$$r(k) = \frac{\sum_{i=1}^k \sigma_i^2}{\sum_{i=1}^N \sigma_i^2}. \quad (3.26)$$

A threshold can be set for the value of  $r(k)$ , e.g. 99.9%.

After POD bases determination, the state space is approximated by the reduced states

$$\begin{bmatrix} \boldsymbol{\rho} \\ \mathbf{u} \\ \dot{\mathbf{m}} \\ \mathbf{T} \end{bmatrix} \approx \begin{bmatrix} V_\rho^T & & & \mathbf{0} \\ & V_u^T & & \\ & & V_m^T & \\ \mathbf{0} & & & V_T^T \end{bmatrix} \begin{bmatrix} \mathbf{a}_\rho \\ \mathbf{a}_u \\ \mathbf{a}_m \\ \mathbf{a}_T \end{bmatrix}. \quad (3.27)$$

Then the governing equations are projected onto different reduced bases, which reveals a coupled reduced system.

As stated before, stability of the reduced order model is generally not guaranteed. To apply the stabilization methods, the reformulated HX model is linearized at some equilibrium points. By checking the sufficient condition in (2.20) for Jacobian matrices, a prior knowledge of stability can be obtained. If not satisfied, the stabilization method based on semidefinite programming is applied. Note that since states are split, and projected onto different bases, the stabilization method cannot be directly used. In this case one of the bases can be modified while fixing the other three. For example, the stabilization method is applied to the temperature basis  $V_T$ , and the resulting reduced model is of the form:

$$\begin{bmatrix} I & & & \mathbf{0} \\ & I & & \\ & & I & \\ \mathbf{0} & & & W_T^T V_T \end{bmatrix} \begin{bmatrix} \dot{\mathbf{a}}_\rho \\ \dot{\mathbf{a}}_u \\ \dot{\mathbf{a}}_m \\ \dot{\mathbf{a}}_T \end{bmatrix} = \begin{bmatrix} V_\rho^T & & & \mathbf{0} \\ & V_u^T & & \\ & & V_m^T & \\ \mathbf{0} & & & W_T^T \end{bmatrix} A \begin{bmatrix} V_\rho & & & \mathbf{0} \\ & V_u & & \\ & & V_m & \\ \mathbf{0} & & & V_T \end{bmatrix} \begin{bmatrix} \mathbf{a}_\rho \\ \mathbf{a}_u \\ \mathbf{a}_m \\ \mathbf{a}_T \end{bmatrix} \quad (3.28)$$

where  $A$  is the Jacobian matrix at a certain equilibrium point, and  $W_T$  is the modified basis from the stabilization algorithm in (2.39).

A reduced order system derived directly from the POD method has a computational complexity issue arising from nonlinearity, though the number of states is reduced. At each iteration, the nonlinear term must be computed with a computational cost that still depends on the full order dimension. In the presence of polynomial nonlinearities, the pre-computation technique of the POD projection is still applicable

for dimension reduction by expanding the high order polynomial. However, the standard POD approach does not admit the sort of pre-computation for general equations involving non-polynomial nonlinearities, such as the heat exchanger model in this work. The DEIM approximation is applied to the reformulated HX model to further improve the computational efficiency. The DEIM method was originally proposed to approximate nonlinear systems arising from finite difference (FD) discretization of partial differential equations. However, the method could be easily adopted to finite volume discretization in this study. Similar to splitting the system trajectories *snapshots*, the nonlinear function *snapshots* are split into four groups based on governing equations. Then interpolation indices are constructed for each group of equations. As shown in (2.56), the DEIM approximation error bound is indicated by the singular values of the snapshot matrix. After decomposing the nonlinear functions snapshot matrix, the ratio of energy captured by the POD basis (3.26) can also be adopted here to determine the number of interpolation points. During the online simulation, only certain governing equations at the interpolation indices are formed and evaluated,

$$\hat{\mathbf{f}} = P^T \mathbf{f} \quad (3.29)$$

where  $\hat{\mathbf{f}} \in \mathbb{R}^m$  represents the set of equations being selected, and  $\mathbf{f} \in \mathbb{R}^N, m < N$  represents all the governing equations including mass, energy and momentum balances.

Procedures of the proposed model order reduction framework is summarized in Fig. 3.3.

### 3.4 Refrigerant Thermodynamic Properties Evaluation

Significant computational requirements for simulating vapor compression system models are associated with evaluation of thermodynamic properties. For example, when a heat exchanger is modeled using a finite volume method, a number of properties or their partial derivatives with respect to inputs have to be calculated for all control volumes of a refrigerant and for each time step. Therefore, reducing the com-

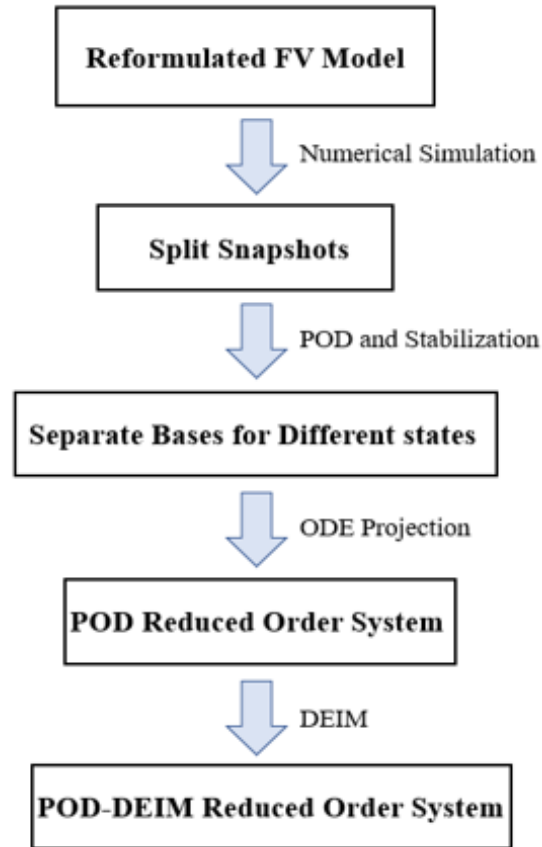


Fig. 3.3. Nonlinear model order reduction framework.

putation time of evaluating thermodynamic properties is particularly important for transient models. The NIST RefProp database [44] and the open-source property library CoolProp [45], are widely used tools for the evaluation of refrigerant properties. However, due to the nature of solving the implicit Equations of State (EOS) which requires numerical iterations, the computational time for a dynamic VCC simulation with direct use of RefProp or CoolProp can be significant [46]. Various approaches have been developed based on curving-fitting and look-up tables [19, 47, 48], but these interpolation-based methods are numerically sensitive to the resolution of a thermodynamic property table due to the computational time to search for the nearest points. On the other hand, the reformulated heat exchanger model uses refrigerant density and internal energy as a pair of independent properties, and other thermodynamic

properties like pressure and temperature need to be calculated from them. However, it is not straightforward to do this in the object-oriented modeling languages like Modelica. Therefore, a fast property evaluation scheme based on artificial neural networks (ANN) is proposed in this work. Training data is generated from RefProp. To the interest of this work, the developed regression model takes inputs density and internal energy, and calculates the output pressure or temperature.

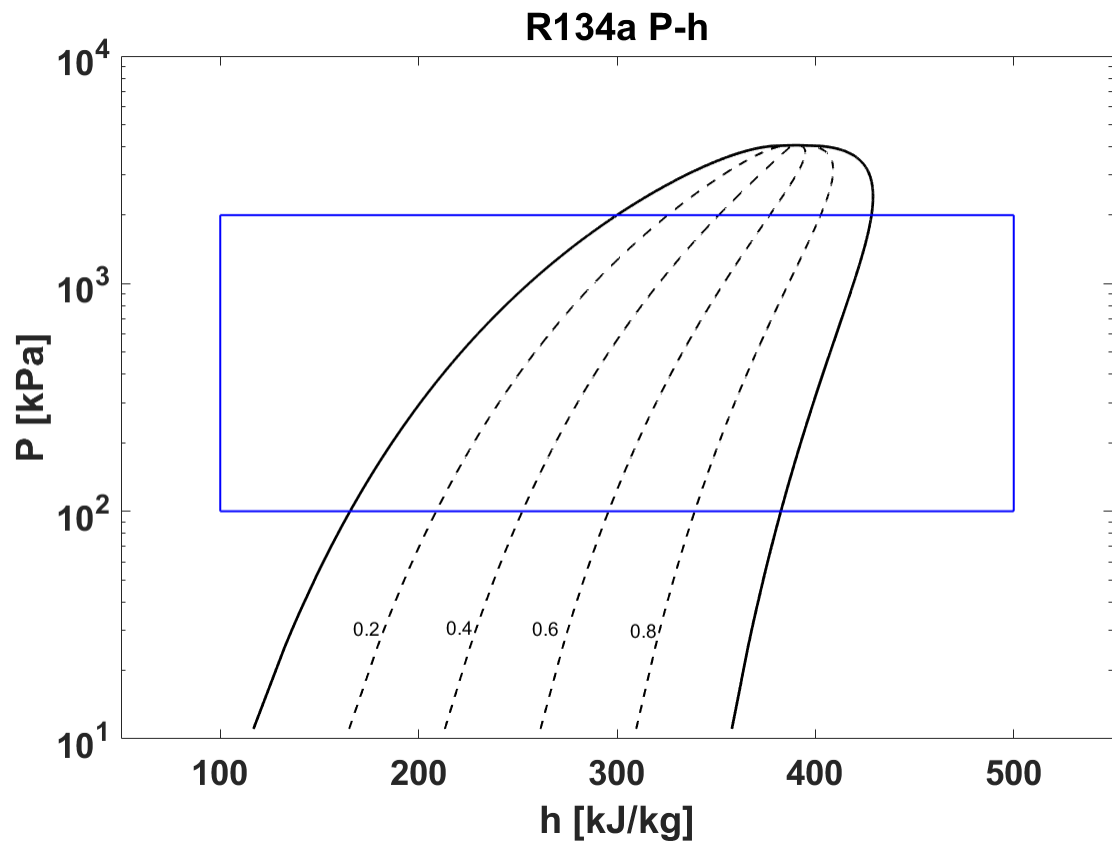


Fig. 3.4. Calculation Bounds of R134a on P-h diagram

Firstly, the domain of interest for a subcritical VCC simulation which uses R134a as a working fluid is specified (Fig. 3.4). The upper and lower bounds of pressure are 20 bar and 1 bar, respectively. The values of 100 kJ/kg and 500 kJ/kg were selected as enthalpy bounds, which covers typical operating conditions of the VCC system

considered in this work. Then the domain is mapped to density and internal energy fields as shown in Fig. 3.5.

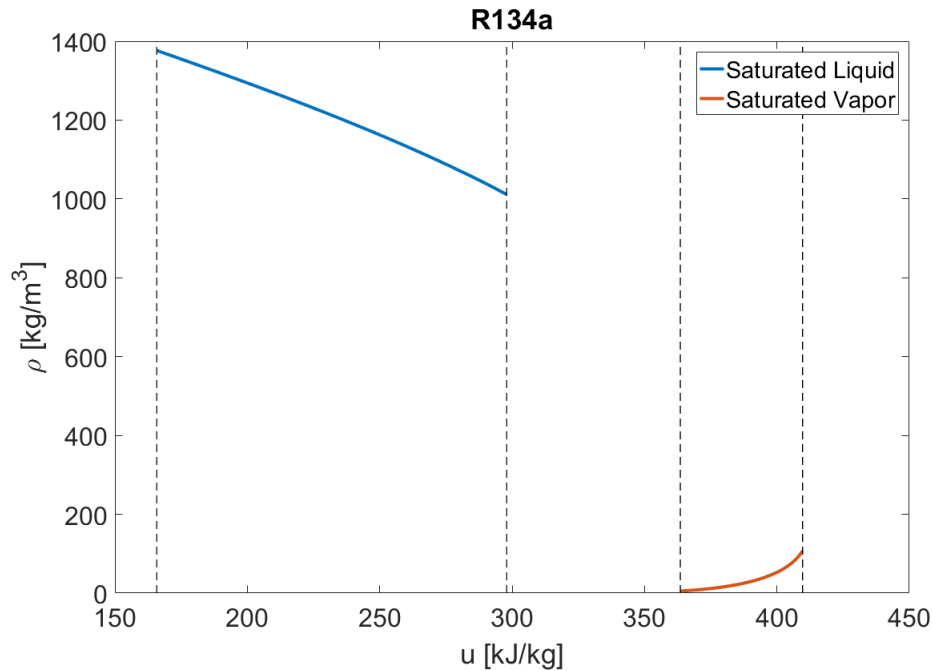


Fig. 3.5. Calculation domain of R134a on  $\rho - u$  diagram

When a pair of state inputs comes, it is first classified into a phase region (liquid, two-phase, vapor). During this process, internal energy is used as the primary axis. For example, when the input internal energy is less than the minimum of the saturated liquid properties, it will be classified into the liquid phase. In other cases, when it is within the range of saturated lines (saturated liquid or vapor), a saturated density is calculated by a logistic regression model

$$\rho_{\text{sat}} = f(u) = c_1 + \frac{c_2}{1 + e^{(a_1 u + a_2)}} \quad (3.30)$$

and then compared with the input density.

Once the phase region is identified, a regression model for that phase is called to calculate pressure or temperature. The model for each phase region taking inputs density and internal energy is a shallow neural network model containing one hidden

layer as shown in Fig. 3.6. For example, when using refrigerant density and internal energy as inputs, the input layer is fully connected with the hidden layer, and three hidden units with a sigmoid activation are applied. The model is trained using the MATLAB Feedforward Neural Network tool. Models for calculating refrigerant pressure and temperature are developed. Then enthalpy can be obtained from the inputs and pressure,

$$h = u + \frac{P}{\rho} \quad (3.31)$$

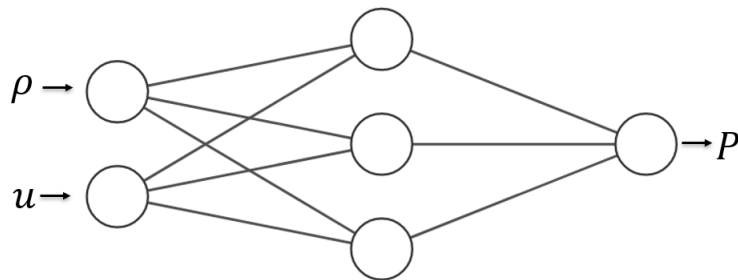


Fig. 3.6. Neural Network architecture for calculating thermodynamic properties

## 3.5 Cycle Model Implementation

### 3.5.1 Object-oriented Modeling with Modelica

Modelica is an object-oriented modeling language for complex and multi-domain physical systems. It has been used to model thermo-fluid systems since the early stage of language development. Though there are some transient modeling tools available in Matlab/Simulink, such as the Thermosys Toolbox [49], a larger class of simulation packages for thermo-fluid systems has been developed based on Modelica, and the Modelica-based modeling approach has demonstrated great potential in the dynamic modeling of HVAC systems in the past decade [22]. It offers some desirable features to address challenges in modeling HVAC equipment, due to the multi-physical and highly nonlinear characteristics. The Modelica language is object-oriented, which

facilitates code reuse, and the modeling effort can thus be considerably reduced. In addition, it is equation-based and supports acausal modeling. Equations are used in Modelica for modeling of the physical phenomena. No particular variable needs to be solved manually, and the calculation order of equations is not specified, because the system is solved simultaneously, and Modelica can decide it automatically. Traditional modeling tools are block-based, and thus require a significant effort to manually rewrite equations into explicit form. The block diagram simulation platforms such as Simulink are built on components with fixed input-output relations [1], but this does not reflect relations of physical variables. For large and complex systems of ordinary differential equations (ODE), differential-algebraic equations (DAE), using Modelica can significantly save the time of model development. Generally, dynamic HVAC systems consist of a set of ODEs and DAEs, and different components are connected by an implicit relation. The implicit equations can be handled efficiently by acausal modeling implementation in Modelica, thus developers can focus more on the underlying physics. Furthermore, Modelica-based simulation tools such as Dymola provide a rich library of numerical solvers that are developed and updated by applied mathematicians, such as DASSL and Radau IIa. In addition, Dymola which is a Modelica-based simulation environment, performs a pre-processing model translation to further improve the solver efficiency, that leads to robust numerical simulations [50].

In terms of simulation of dynamic HVAC systems, several Modelica-based libraries have been developed and are utilized in application, e.g. the ThermoFluid (2003), the TIL (2008), the Air Conditioning Library (2014).

To model a VCC component in Modelica, all balance equations can be provided in their natural form. Then different components are connected by the specific class “connector” in Modelica language. The connector variables are selected such that connected components fulfill the model balance (the same number of unknowns and equations). For example, when a heat exchanger and compressor are connected by

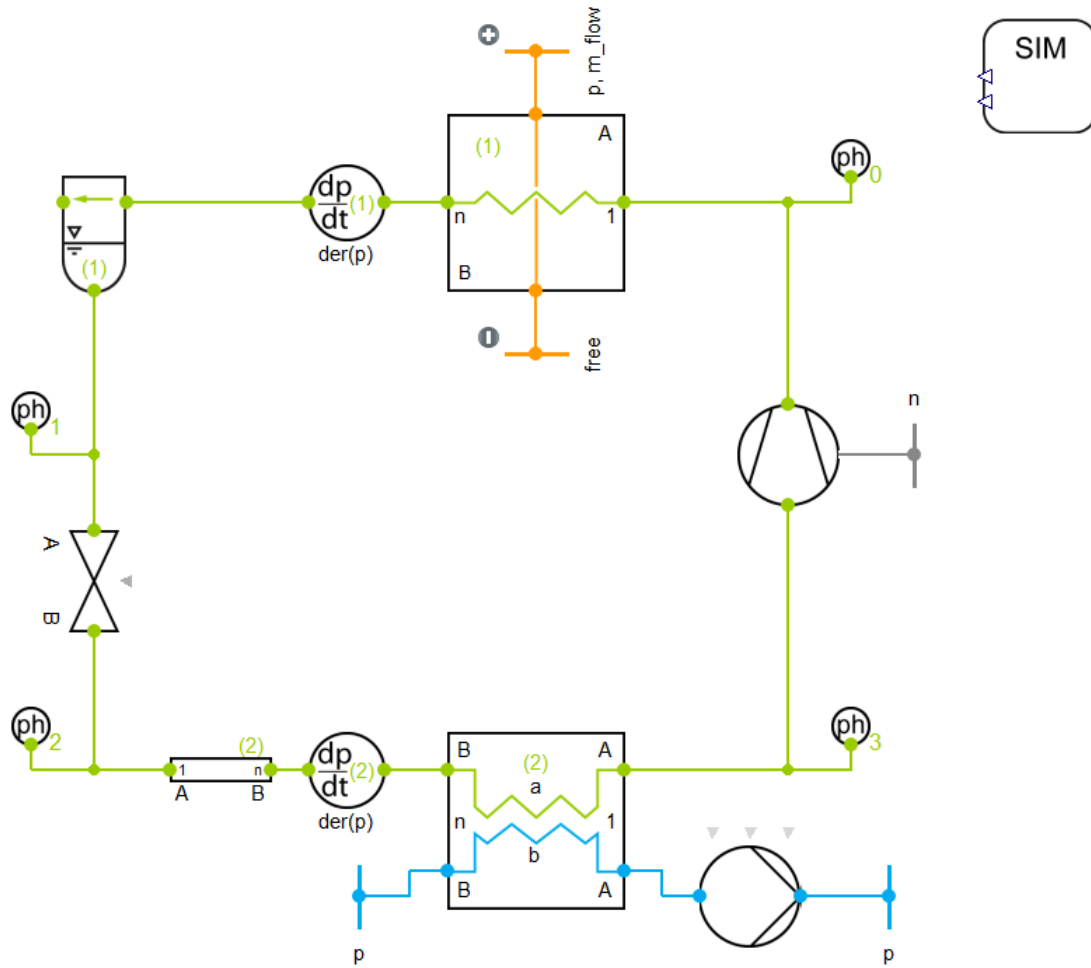


Fig. 3.7. Vapor compression system in TIL library.

variables pressure and mass flow rate inside connectors, Modelica will generate additional balance equations:

$$P_{hx} = P_{comp} \quad (3.32)$$

$$\dot{m}_{hx} + \dot{m}_{comp} = 0 \quad (3.33)$$

where  $hx$  denotes the heat exchanger, and  $comp$  denotes the compressor. It indicates that potential variables (pressures) of the connectors are identical, and the sum of flow variables (mass flow rates) is 0. Fig. 3.7 shows the graphical interface of a typical

VCC system in the Modelica TIL library. Components including heat exchangers, compressor, expansion valve, tanks, pump are connected by different connectors corresponding to different flow paths, e.g. refrigerant, air, water. The refrigerant flow path connecting heat exchangers, compressor and valve forms a closed cycle, and equations within these components are solved simultaneously. For efficient integration, the numerical solver will rearrange all the equations to a block lower rectangular form using a symbolic manipulation and a special algorithm from the graph theory.

Initialization of large nonlinear systems is always challenging for dynamic modeling. It is also a difficult issue in the Modelica-based simulation. As described earlier, system components are represented by DAEs in Modelica. Solving DAEs requires a consistent set of initial conditions, which may be difficult to satisfy. If the guess values of initial conditions are rather inaccurate or far from the true solutions, the model may diverge, or converge to an undesired solution. Some techniques can be used to deal with this issue, such as setting bounds for variables, scaling states variables, and avoiding discontinuities.

### 3.5.2 Reduced Cycle Model

Within the typical four-components vapor compression system consisting of condenser, evaporator, compressor and expansion valve, because the dynamics of compressor and expansion device generally evolve on an order of magnitude faster than those of heat exchangers, these mass flow devices are modeled with quasi-static relationships, and then coupled with dynamic heat exchanger models. For the purpose of reduced order modeling of a VCC, the model reduction approaches developed in this work are applied to the reformulated HX model to generate nonlinear reduced order HX models (NL-ROM). After that, they are coupled with the quasi-static models to complete a reduced order cycle. The overall process is depicted in Fig. 3.8.

Implementing the reformulated HX models with quasi-static models is not straightforward. The full VCC model needs to be adjusted to handle connections between

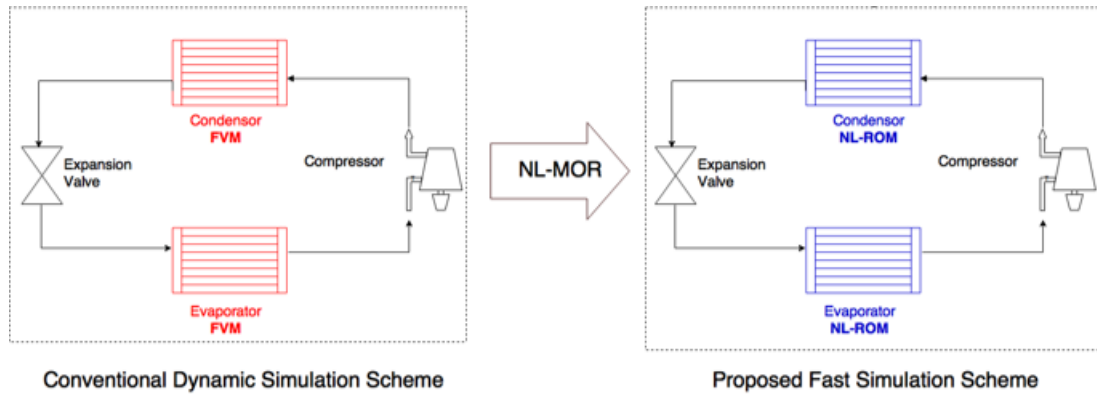


Fig. 3.8. Generating reduced order VCC model.

them. In the conventional VCC model with the standard FV heat exchanger models, the condensing and evaporating pressures are dynamic states, and are outputs of HX models. Then they are fed into compressor and expansion valve models to calculate the refrigerant mass flow rates. However, since the reformulated HX model is discretized with a staggered grid, and applies outlet pressure as a boundary condition, condensing and evaporating pressures are no longer inputs for the empirical models of the compressor and expansion valve. To ensure the model balance, HX outlet mass flow rates as well as pressures calculated at the inlet (first volume) are sent into quasi-static models, and the HX outlet pressure is found to match the quasi-static model outputs by iterations. It also illustrates the advantage of the acausal modeling concept of the Modelica language. Though the resulting system is balanced, it involves implicit iterations at the system level. If implemented by Modelica, the four components can be connected by connectors containing pressures as potential variables, then the solver will handle the internal iterations automatically. Though it is possible to do this in the conventional modeling tools based on input-output blocks, much more development time and effort on determining calculation orders is needed. For those components containing clear input-output relations, such as the controller and TXV bulb, it is also convenient to model them as blocks in Modelica.

### 3.5.3 Numerical Treatments

Simulations of large and complex systems are often challenged by numerical issues, such as chattering and increased stiffness that can slow down or lead to failed integration. The discontinuities in model representations are major sources of numerical issues. In VCC modeling, typical discontinuities occur in computing heat transfer coefficients. When different heat transfer correlations are applied for different phase regions (liquid, two-phase, vapor), potential discontinuities may exist at the saturation states. Qiao [51] described the oscillation caused by discontinuities in heat transfer coefficient between two-phase and vapor states. Generally the heat transfer coefficient of the two-phase region is much higher than the vapor phase. When refrigerant of a control volume within the evaporator is in the two-phase region, it will be heated up to become a superheated vapor. However, once it becomes vapor, the heat flow decreases significantly due to a much smaller heat transfer coefficient. When considered in combination with pressure changes, the state of refrigerant may change back to the two-phase, and this process would repeat over again, which results in chattering. Chattering may occur when discontinuities exist in the model. Once it occurs, the simulation easily gets stuck at the current step, and does not make progress over time.

Discontinuities exist in other subroutines or models as well. Recall that the proposed thermodynamic property evaluation scheme is composed of two steps. First the input states are classified into a phase region (liquid, two-phase, vapor) by comparison with the saturated properties. Then a regression model within the determined phase region is called to calculate the output. Discontinuities occur at the boundary of each phase region, since different regression models are utilized crossing the boundary. Besides chattering, this may lead to increased stiffness of the model due to the large variation of refrigerant density around the saturated liquid line. Generally speaking, any switched model representation based on IF-THEN algorithms leads to inherited discontinuities. One of the remedies to avoid this is to smooth the disconti-

nities by numerical treatments. For example, when the solution has a discontinuous jump at the switching boundary due to IF-THEN rules, a function can be manually created to connect two models. This is equivalent to smooth a step change by a polynomial function as shown in Fig. 3.9. In the Modelica language, the built-in function `Fluid.Utilities.regStep` can be used to achieve this.

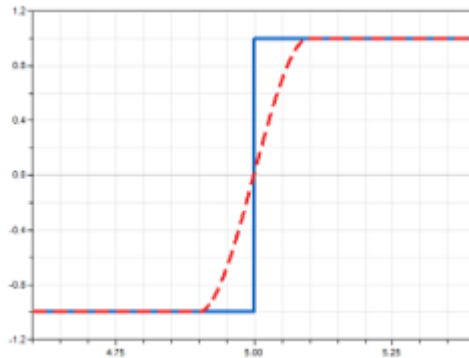


Fig. 3.9. Smoothing a step change by a polynomial function.

In addition, highly nonlinear sub-models such as the heat transfer correlations and thermodynamic property calculations can bring computational challenges in solving a VCC model, when these nonlinearities are coupled into the overall cycle model. Laughman and Qiao [41] showed that cycle models that incorporate nonlinear heat transfer correlations and frictional pressure losses may exhibit problematic dynamics that result in slow execution times and may demonstrate nonphysical behavior, such as oscillations. They proposed adding a low-pass filter to decouple the nonlinear behavior from the other state variables. Suppose that the heat transfer coefficient is a function of the current refrigerant state. A reference value is calculated by the conventional heat transfer correlation, and then the true value is obtained by a low-pass filter.

$$\hat{\alpha} = f(\rho, u, \dot{m}) \quad (3.34)$$

$$\frac{d\alpha}{dt} = \frac{1}{\tau}(\hat{\alpha} - \alpha) \quad (3.35)$$

where  $\hat{\alpha}$  is the reference value obtained from a correlation,  $\alpha$  is the true value used in energy balances, and  $\tau$  is the time constant. This approach is expected to reduce the sensitivity of the system to large gradients, since now the heat transfer coefficient will depend on its value of the previous step. The time constant  $\tau$  should be chosen to make it faster than other system dynamics, so that it will not change the system response.

This method can be extended to reduced order models in the current work. Recall that the reduced order HX models are coupled with quasi-static models of the compressor and expansion valve to form a reduced cycle. At each time step, the dynamics of reduced states are evaluated then transformed back to the original state space to complete the cycle, since the reduced states do not have physical meaning. However, this process involves nonlinear maps. Consider the reduced HX states  $\mathbf{a}$ , and the reduced basis  $V$ , the original states can be obtained by projecting back to the state space,

$$\mathbf{x} = V\mathbf{a} \quad (3.36)$$

where  $\mathbf{x}$  are states consisting of refrigerant density, internal energy, mass flow rates, and tube and secondary fluid temperatures. Refrigerant thermodynamic states at the HX inlet and outlet should be mapped to other properties, e.g. pressure and temperature, that are used in the quasi-static compressor and valve models.

$$(P, h) = g(\rho, u) \quad (3.37)$$

where  $g()$  is the nonlinear map of the thermodynamic property calculations. At the overall cycle level, reduced HX models are coupled with quasi-static models by the projection and these nonlinear maps, which can impose significantly computational challenges. Therefore, the method of low-pass dynamics is adopted to decouple the closure relations of component models. Outputs from the reduced HX models are considered as reference values,

$$\dot{\mathbf{a}} = f(\mathbf{a}, \mathbf{u}) \quad (3.38)$$

$$\hat{\mathbf{y}} = g(\mathbf{a}) \quad (3.39)$$

where  $\mathbf{a}$  denotes the reduced states,  $\mathbf{u}$  denotes the inputs, and  $\hat{\mathbf{y}}$  denotes the outputs, such as the outlet pressure and temperature. In the connection between HX models and the quasi-static models, the true values are obtained by

$$\frac{d\mathbf{y}}{dt} = \frac{1}{\tau}(\hat{\mathbf{y}} - \mathbf{y}) \quad (3.40)$$

where the parameter  $\tau$  should be tuned to be faster than the system dynamics, but still effective in decoupling component models.

## 4. MODEL VALIDATIONS

### 4.1 Experimental Facility

Reduced order modeling approaches are developed for a centrifugal chiller system. Simulation results are compared with experimental data over a wide range of operating conditions and transients. The chiller is a 300-kW centrifugal system. Cycle components include a shell-and-tube condenser, a shell-and-tube evaporator, a single stage centrifugal compressor, a thermostatic expansion valve, and a local controller adjusting the compressor's inlet guide vanes for capacity control. The refrigerant used in the system is R134a, and the secondary fluid is water. A schematic of the refrigerant and water flow paths is shown in Fig. 4.1. Besides the main flow path, there

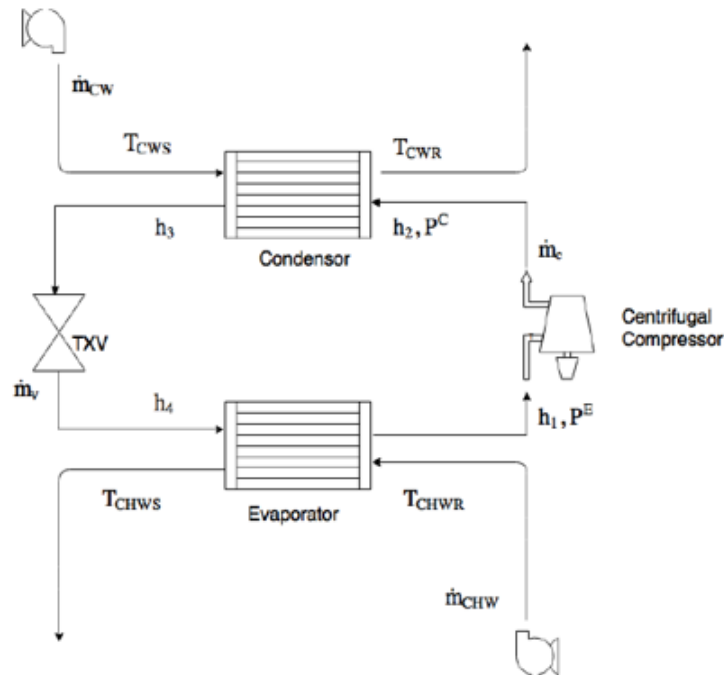


Fig. 4.1. Schematic of chiller system.

is a bypass cooling line that is tapped at the exit of the condenser. This line carries liquid refrigerant to the motor, and then used to cool the motor and transmission oil. After that, the heated refrigerant is returned to the main refrigerant stream at the evaporator inlet. Fig. 4.2 shows the refrigerant flow paths.

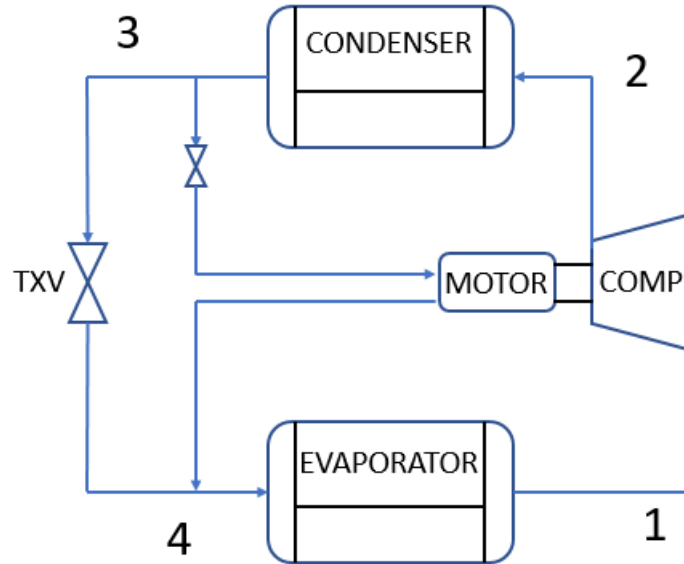


Fig. 4.2. Refrigerant flow schematic.

Transient data were collected at 10s intervals, covering the start-up, and a sequence of different operating conditions driven by changes in the condenser and evaporator water inlet temperatures, and chilled water set-point temperature.

## 4.2 Model Development

### 4.2.1 Compressor

The compressor is a single-stage centrifugal machine with variable inlet guide vanes to adjust the refrigerant mass flow rate. It is driven by a constant-speed electric motor. A quasi-static model was developed by [10] including a maximum capacity map, and the actual mass flow rate correction.

A maximum capacity map was built assuming that the compressor is operating with wide-open vanes. The maximum mass flow rate is computed from the given boundary conditions. Then the actual mass flow rate is obtained by applying a vane-position correction to the maximum flow. The computed actual flow is used in the model to estimate the exit condition and motor power. A second order regression model taking discharge pressure, suction pressure, and suction temperature as inputs, was used to compute the maximum capacity flow rate,

$$\dot{m}_{max} = c_0 + c_1 P_e + c_2 P_c + c_3 T_e + c_4 P_c P_e \quad (4.1)$$

where  $P_c$  denotes the discharge pressure,  $P_e$  denotes the suction pressure, and  $T_e$  denotes the suction temperature. A flow rate correction in terms of the vane-position was integrated into a factor  $\gamma$ , and the actual mass flow rate is calculated by:

$$\dot{m}_c = \gamma \dot{m}_{max}. \quad (4.2)$$

Calculation of the factor  $\gamma$  will be discussed in the controller model section. The actual flow rate is used in other quasi-static models, which were built from steady-state data of the test stand. To estimate the motor power and heat loss, the polytropic efficiency was regressed as a second order polynomial in the volumetric flow rate  $\dot{V}$  (m<sup>3</sup>/s) and the polytropic work  $W_p$  (kJ/kg),

$$\eta_p = a_0 + a_1 \dot{V} + a_2 \dot{V}^2 + a_3 W_p + a_4 W_p^2. \quad (4.3)$$

The polytropic compression work is calculated by:

$$W_p = (P_c v_2 - P_e v_1) \frac{\ln(P_c/P_e)}{\ln(P_c v_2/P_e v_1)} \quad (4.4)$$

where  $v_2$ ,  $v_1$  are the refrigerant specific volumes at the compressor outlet and inlet (see Fig. 4.2), respectively. Under the assumption of adiabatic compression, a constant motor electro-mechanical efficiency  $\eta_{em}$  was computed from the steady-state data.

Then the motor power and losses are calculated as:

$$P_{mo} = \dot{m}_c \frac{W_p}{\eta_p \eta_{em}} \quad (4.5)$$

$$\dot{Q}_{loss} = (1 - \eta_{em}) P_{mo}. \quad (4.6)$$

Finally, the compressor exit enthalpy is estimated from an energy balance:

$$P_{mo} = \frac{\dot{m}_c(h_2 - h_1)}{\eta_{em}}. \quad (4.7)$$

Note that solving the compressor model requires numerical iterations, because the undetermined outlet condition is used in calculating the compression work in (4.4). Bendapudi [10] set a guess value of the exit enthalpy to compute a specific volume with the discharge pressure  $v_2 = f(h_{guess}, P_c)$ . After calculating the enthalpy from (4.7), it is compared with the guessed value. This process is repeated until the error is below a predefined tolerance. In the Modelica-based simulation environment, the solver naturally handles the internal iteration of the compressor model, using acausal modeling.

There exists a control logic that prevents the compressor motor current from exceeding the rated amperage. This feature is modeled by a percentage of the rated amps of the motor, and the quantity is referred to as the “RLA”. It was regressed from the prediction of motor power:

$$\text{RLA} = b_0 + b_1 P_{mo} + b_2 P_{mo}^2. \quad (4.8)$$

When it is below the limit, the refrigerant mass flow rate obtained from the controller and the maximum capacity map is the input to the quasi-static model, and the motor power is an output. When the limit is reached, the motor power is solved at the limit current from (4.8), and is imposed as an input, then the mass flow rate and discharge enthalpy are computed as outputs.

#### 4.2.2 Expansion valve

The thermostatic expansion valve (TXV) adjusts the refrigerant flow rate into the evaporator, to maintain a certain refrigerant superheat at the evaporator exit. The valve increases or reduces the flow area thus altering the amount of refrigerant fed into the evaporator. The response time of the valve depends on how fast the sensing

bulb reacts to a temperature change. Refrigerant inside the bulb (R500) was modeled by a simplified lumped-capacitance element,

$$C_b \frac{dT_b}{dt} = T_e - T_b \quad (4.9)$$

where  $C_b$  is a coefficient incorporating the effects of refrigerant mass in the bulb, and heat transfer resistance of the bulb body. It was estimated from the data using the superheat response time during load-change transients. The dynamics of the bulb temperature are included in the system dynamics, so the temperature can be solved at every time step. Then it is used to calculate the bulb pressure, since the refrigerant inside the bulb is always in a two-phase condition. The lift of the valve is computed by the pressure difference,

$$y = k_{spring}(P_b - P_e - \delta P_{min}) \quad (4.10)$$

where  $\delta P_{min}$  is the minimum pressure difference required to open the valve. The flow area of the valve is regressed as:

$$A_v = a_0 y + a_1 y^2. \quad (4.11)$$

Finally the refrigerant mass flow rate can be determined by the orifice equation:

$$\dot{m}_v = C A_v \sqrt{2(P_c - P_e)/v_3} \quad (4.12)$$

where  $v_c$  is the refrigerant specific volume at the condenser outlet, and  $C$  is a constant coefficient.

Recall that a part of the refrigerant flow from the condenser outlet flows through a bypass line ( $\dot{m}_{cl}$ ) for cooling the compressor motor and the transmission oil, and returns to the evaporator inlet. There is an orifice in the motor cooling line that drops the pressure of the refrigerant from the condensing pressure to the evaporating pressure, so that refrigerant pressure at the evaporator inlet is balanced. With the assumption that the compressor is adiabatic, all motor losses are added to the cooling line. Thus the refrigerant enthalpy at the evaporator inlet can be obtained by:

$$\dot{Q}_{loss} = (\dot{m}_v + \dot{m}_{cl})(h_4 - h_3). \quad (4.13)$$

### 4.2.3 Controller

The local controller for the compressor inlet guide vane was modeled by a simple step-and-wait approach. The controller samples the chilled water temperature at fixed intervals. Based on the difference from the set-point water temperature, the control action of incremental opening or closing of the inlet guide vane is determined. The factor  $\gamma$  (bounded between 0.05, to represent fully closed status, and 1.0, to represent fully open.) is updated when the sampling event is triggered, thus it is convenient to model it as a discrete block.

### 4.2.4 Heat Exchangers

Both the condenser and evaporator are 2-pass shell-and-tube heat exchangers, with water as the secondary fluid. The tubes are made of copper and the shell is made of steel. The water flows in the tubes and the refrigerant flows outside them. On the shell side, the refrigerant typically enters at the top or the bottom of the shell, depending on the condenser or evaporator application. Detailed physical geometry of the heat exchangers are provided in [5]. Flow patterns inside the heat exchangers are complicated, and is difficult to model. Since the refrigerant temperature as well as the water temperature vary more significantly along the length of the heat exchanger than across, it can be simplified to a pure counter flow pattern for modeling purposes. The condenser and evaporator are modeled by the reformulated FV model developed in Chapter 3. 15 control volumes are used for both heat exchangers, resulting in HX models of 75 states.

Correlations used for determining the heat transfer coefficients are introduced in [5], however, they are simplified in the current heat exchanger models to improve the numerical robustness of the overall model. On the refrigerant side, the heat transfer coefficients in the superheated region and subcooled region are regressed as a second order polynomial of refrigerant mass flow rate and temperature (Fig.

4.3). Similarly, the water side heat transfer coefficient is regressed as a first order polynomial of water temperature and mass flow rate (Fig. 4.4).

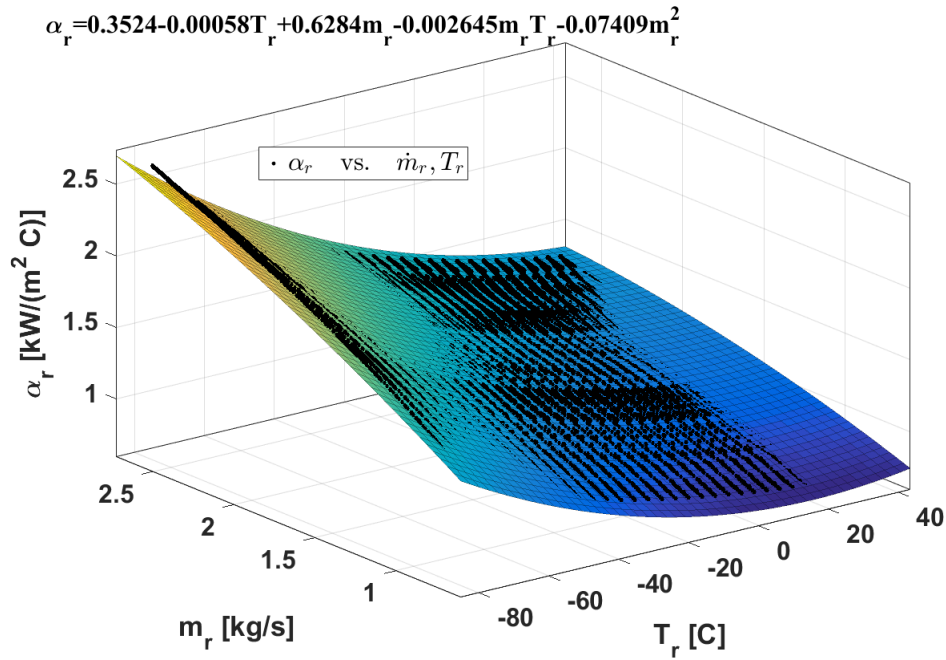


Fig. 4.3. Refrigerant single-phase heat transfer coefficient as a function of flow rate and temperature .

In terms of the two-phase heat transfer coefficients (condensation and boiling), polynomial regressions cannot accurately predict outputs of the empirical correlations, due to their high nonlinearities. Laughman et al. [52] studied the application of nonparametric statistical learning techniques for approximating heat transfer coefficient in dynamic simulation. However, integrating the nonlinear kernel maps potentially increases model complexity, and training the model is time-consuming when the system covers a wide range of operating conditions. Constant nominal values are applied for two-phase heat transfer coefficients in this work, and they are tuned to match the steady-state heat transfer rates [1]. Unlike the original heat transfer correlations, the current model from simplification avoids evaluating the refrigerant and water transport properties, which can speed up the transient simulations.

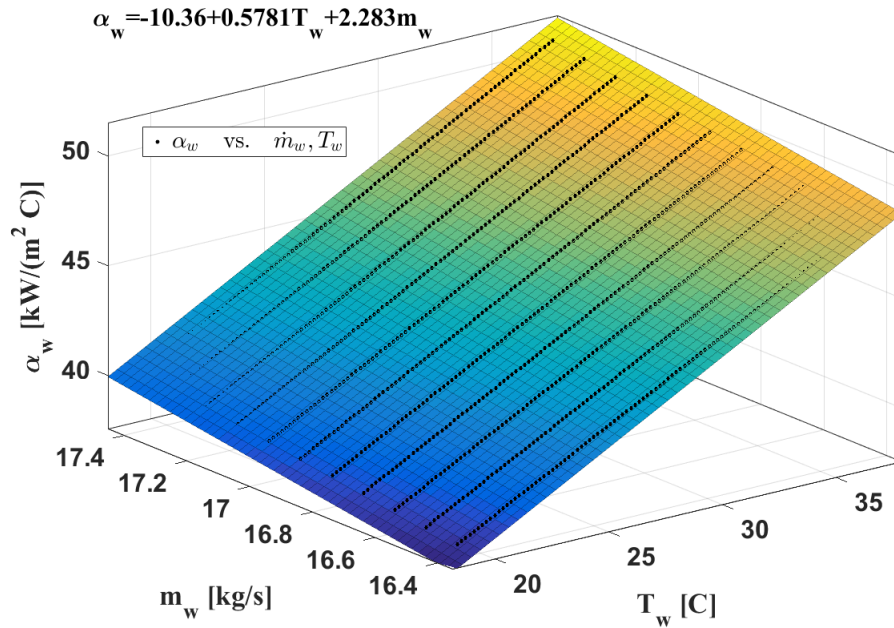


Fig. 4.4. Water heat transfer coefficient as a function of flow rate and temperature .

Reduced order heat exchanger models are generated by the Proper Orthogonal Decomposition and the Discrete Empirical Interpolation Method. The first step is to simulate the reformulated FV model to generate numerical solutions. The model is executed using a pre-defined boundary condition profile to collect snapshots of system trajectories and nonlinear dynamics. To capture the system responses, different combinations of boundary conditions should be fed into the model. Recall that boundary conditions of the HX model consist of the refrigerant inlet mass flow rate and enthalpy, outlet pressure, and water inlet mass flow rate and temperature. The profile is designed to capture step responses of the HX model corresponding to perturbations around some steady-states conditions. An advantage of applying the staggered grid is that the current boundary conditions can be perturbed one by one to identify the response time for a step change, then the input profile is designed to make sure that the system reaches the equilibrium point before the boundary conditions are perturbed again. If the standard FV model applying the refrigerant inlet and outlet

mass flow rates as boundary conditions is used, it will be difficult to decide the time interval length for each perturbation, because whenever they are unbalanced, the system charge dominated by the mass balance changes dramatically over time, and will drive the system to unreasonable states. Snapshots of the condenser and evaporator models are collected around four operating conditions of the chiller system (listed in Table 4.1)

Table 4.1.  
Operating conditions for generating snapshots

<b>Test No.</b>	$T_{set}(C)$	$T_{cwi}(C)$	$T_{ewi}(C)$
1	9.4	29.8	15.9
2	10	29.5	13.8
3	10	29.5	12
4	9.4	24.2	16.3

The reformulated HX model was simulated in Dymola (a Modelica-based simulation tool), and over one million snapshots (states vectors and nonlinear functions vectors) were generated for each heat exchanger. Radau IIa solver was utilized, and the default error tolerance  $1e^{-4}$  was applied. The simulations were completed in 35 minutes. Note that this simulation of collecting snapshots is a one-time task. Once the reduced order models are generated, they can be repeatedly used for control or FDD applications. Reduced order bases were extracted from the snapshots matrix by POD, after splitting the data based on different dynamic states. Applying SVD to each split snapshots matrix, orthonormal bases of dimension  $\mathbb{R}^{15 \times 15}$  (15 control volumes) can be obtained for density, internal energy, mass flow rate snapshots, and a basis of dimension  $\mathbb{R}^{30 \times 30}$  is obtained for the temperatures snapshots. Then the ratio of energy captured by leading singular values to the total energy (3.26) is used to determine dimension of each reduced basis. For the condenser, energy ratio of the states of density, internal energy, interface mass flow rates, tube and water temper-

atures are shown in Fig. 4.5-4.8. The dimension is chosen when the energy ratio is below 0.01%, which means the resulting POD basis vectors capture 99.99% energy of the snapshots. The dimension of the reduced states for each group is listed as follows:

$$\boldsymbol{\rho}_c \approx V_{c,\rho} \mathbf{a}_{c,\rho} \quad \boldsymbol{\rho}_c \in \mathbb{R}^{15}, \mathbf{a}_{c,\rho} \in \mathbb{R}^8 \quad (4.14)$$

$$\mathbf{u}_c \approx V_{c,u} \mathbf{a}_{c,u} \quad \mathbf{u}_c \in \mathbb{R}^{15}, \mathbf{a}_{c,u} \in \mathbb{R}^9 \quad (4.15)$$

$$\dot{\mathbf{m}}_c \approx V_{c,m} \mathbf{a}_{c,m} \quad \dot{\mathbf{m}}_c \in \mathbb{R}^{15}, \mathbf{a}_{c,m} \in \mathbb{R}^8 \quad (4.16)$$

$$\mathbf{T}_c \approx V_{c,T} \mathbf{a}_{c,T} \quad \mathbf{T}_c \in \mathbb{R}^{30}, \mathbf{a}_{c,T} \in \mathbb{R}^9 \quad (4.17)$$

Therefore the reduced order condenser model is of 34 states totally. The reduced order evaporator model was generated in the same way, and the resulting reduced states dimension is listed here:

$$\boldsymbol{\rho}_e \approx V_{e,\rho} \mathbf{a}_{e,\rho} \quad \boldsymbol{\rho}_e \in \mathbb{R}^{15}, \mathbf{a}_{e,\rho} \in \mathbb{R}^9 \quad (4.18)$$

$$\mathbf{u}_e \approx V_{e,u} \mathbf{a}_{e,u} \quad \mathbf{u}_e \in \mathbb{R}^{15}, \mathbf{a}_{e,u} \in \mathbb{R}^9 \quad (4.19)$$

$$\dot{\mathbf{m}}_e \approx V_{e,m} \mathbf{a}_{e,m} \quad \dot{\mathbf{m}}_e \in \mathbb{R}^{15}, \mathbf{a}_{e,m} \in \mathbb{R}^4 \quad (4.20)$$

$$\mathbf{T}_e \approx V_{e,T} \mathbf{a}_{e,T} \quad \mathbf{T}_e \in \mathbb{R}^{30}, \mathbf{a}_{e,T} \in \mathbb{R}^{10}. \quad (4.21)$$

After determining the dimension of POD reduced order models, a similar process was conducted to select interpolation indices for approximating nonlinear functions. Note that the number of snapshot vectors of nonlinear functions are the same as state trajectories vectors, because the data was stored at each time instance during the simulation. Fig. 4.9-4.11 show the SVD analysis of nonlinear function snapshots of the condenser. Since the refrigerant mass balances are linear functions in refrigerant mass flow rates, there is no need to apply the DEIM approximation. The number of refrigerant momentum balances, energy balances, tube and water energy balances are selected if the reduced basis captures 99.9% of the total energy. The final POD-DEIM reduced order condenser and evaporator models are summarized in Table 4.2. Wherein, FOM denotes the full order models, which are the reformulated HX models applying 15 control volumes, and ROM denotes the reduced order models constructed by the proposed POD-DEIM approach. It can be observed that for both HX models,

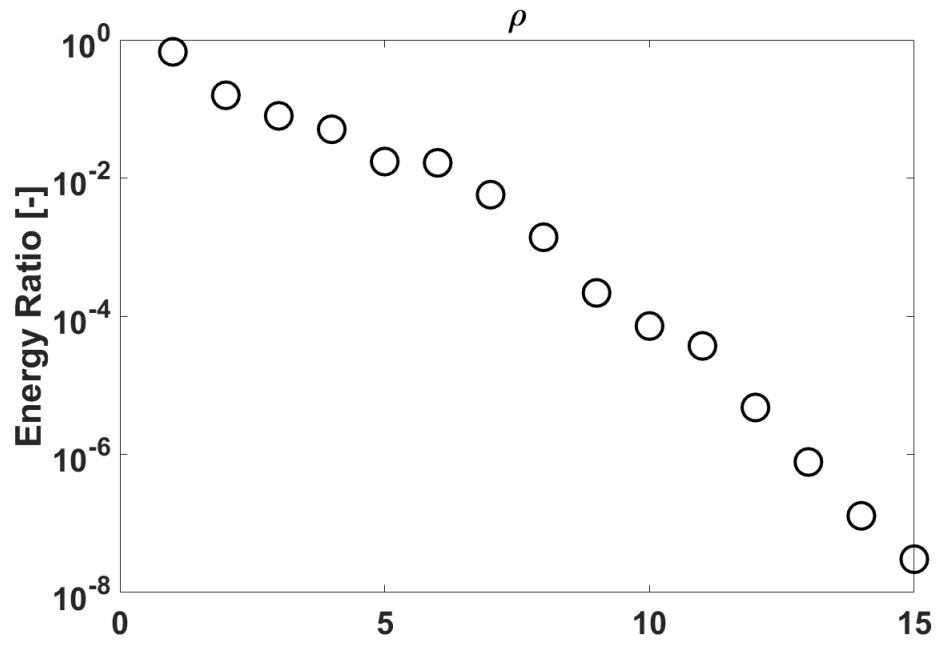


Fig. 4.5. Density snapshots energy ratio.

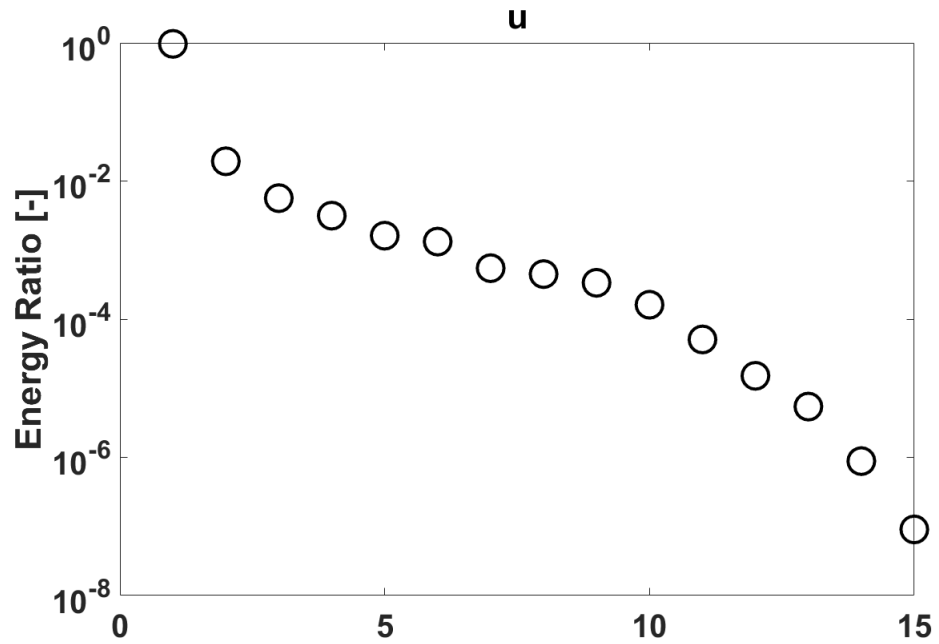


Fig. 4.6. Internal energy snapshots energy ratio.

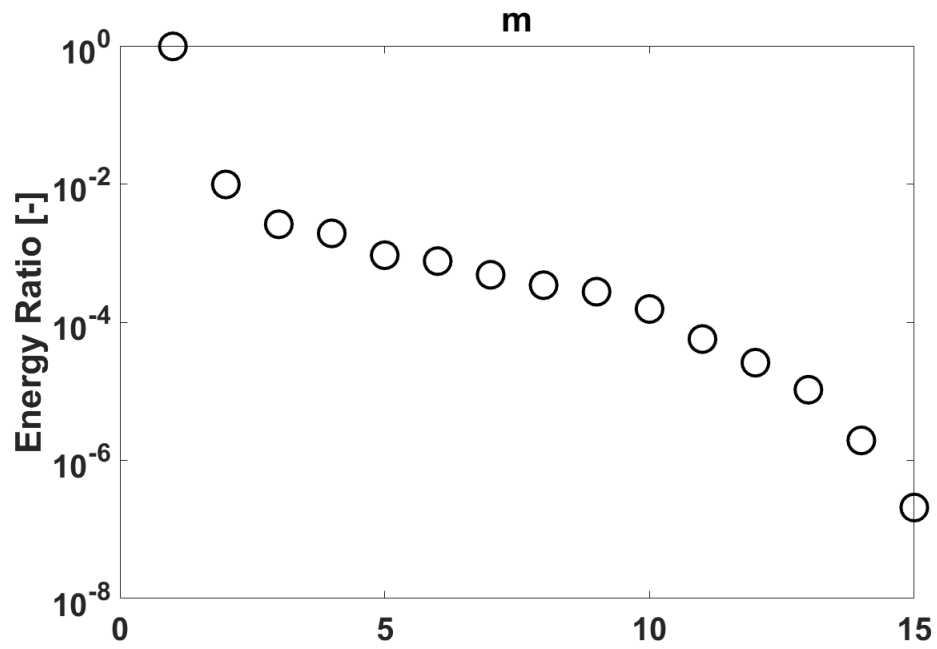


Fig. 4.7. Mass flow rate snapshots energy ratio.

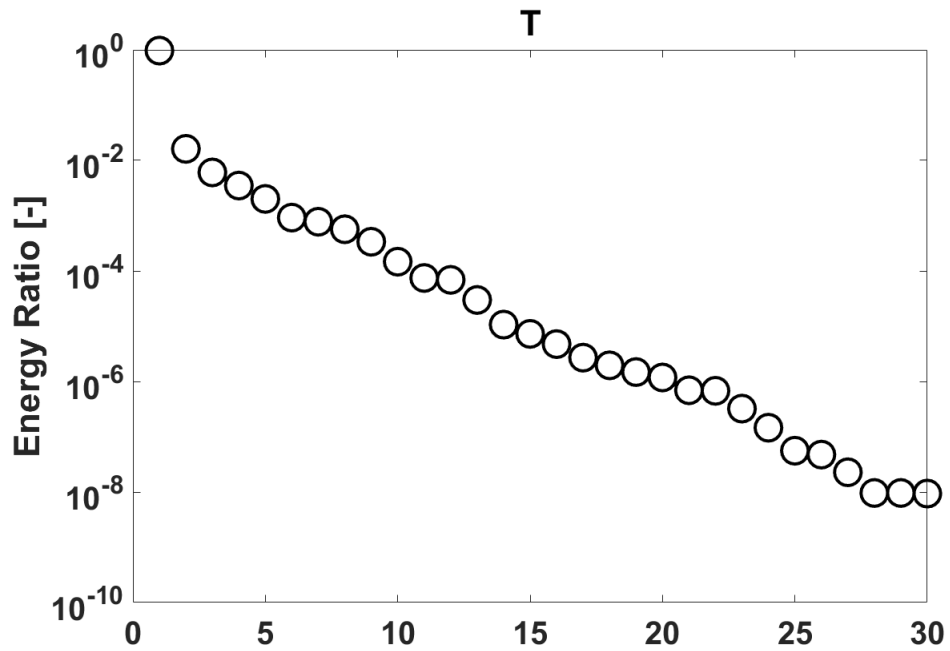


Fig. 4.8. Temperatures snapshots energy ratio.

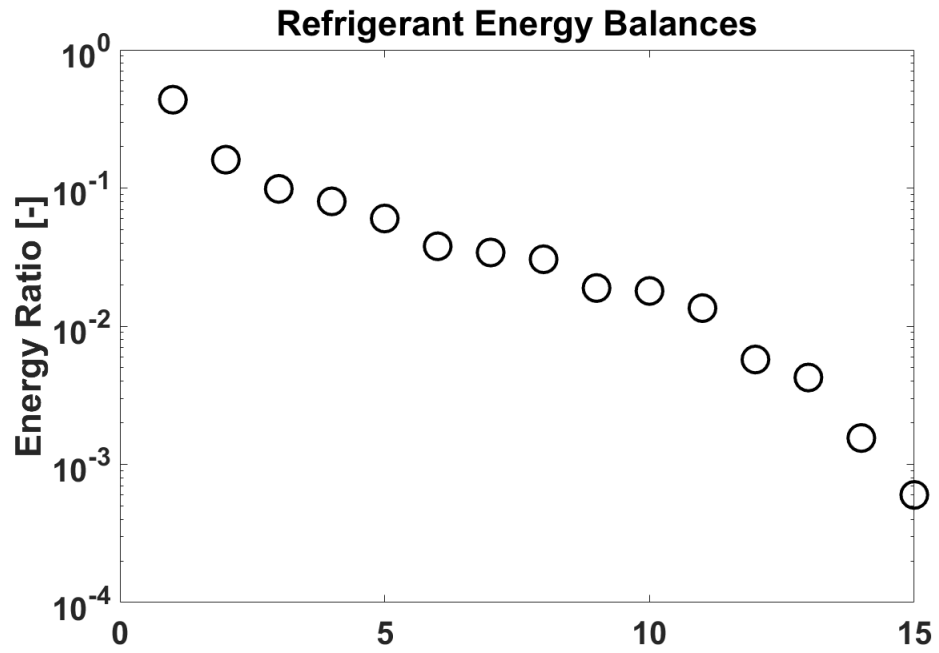


Fig. 4.9. Refrigerant energy balances snapshots energy ratio.

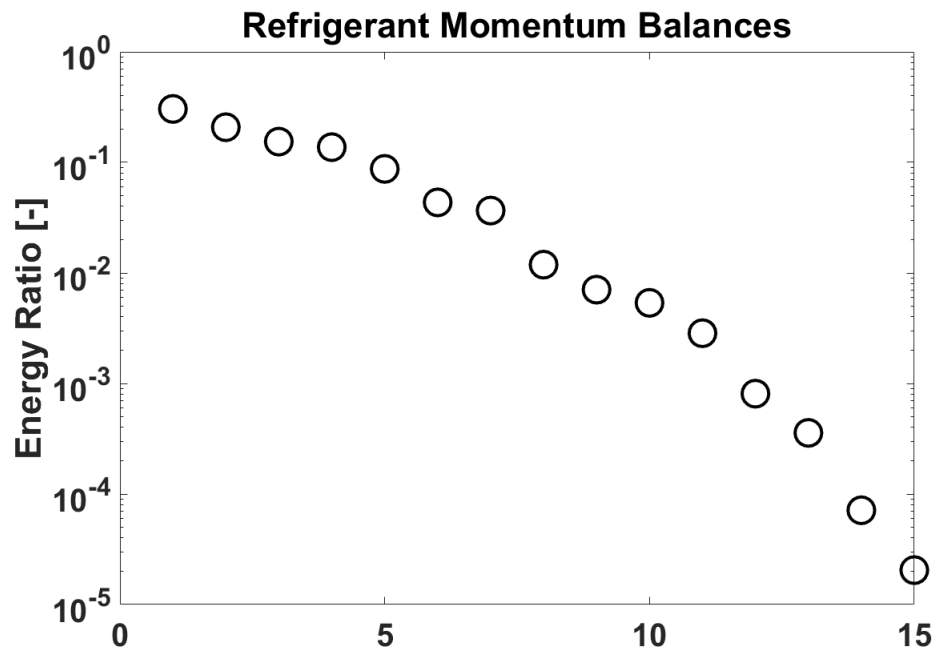


Fig. 4.10. Refrigerant momentum balances snapshots energy ratio.

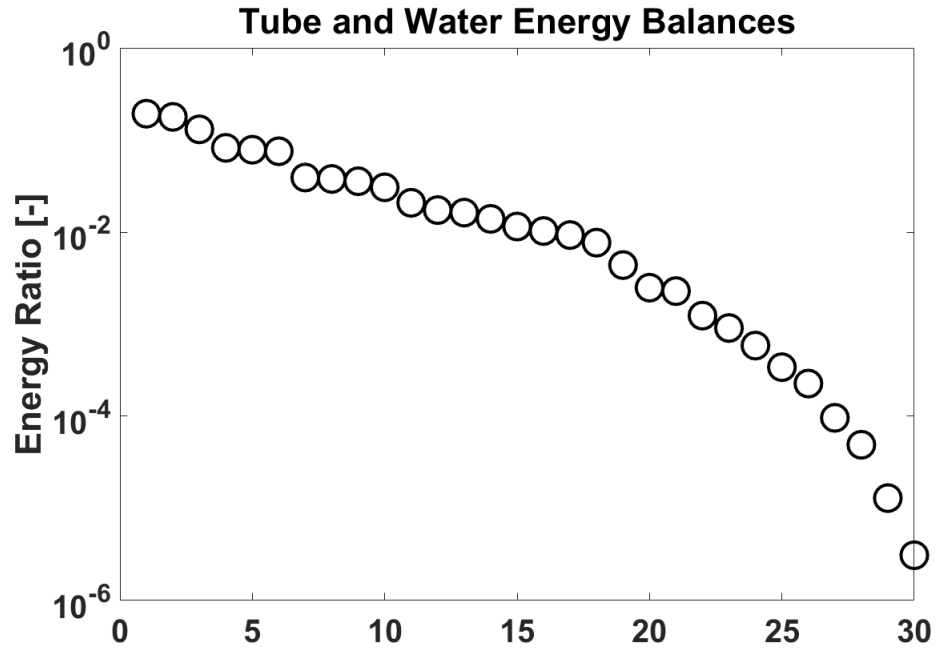


Fig. 4.11. Tube and water energy balances snapshots energy ratio.

more than half of the states were reduced by POD analysis, and nearly one third of the ODEs were eliminated by the DEIM scheme.

Table 4.2.  
Reduced order condenser and evaporator models

HX	FOM No. States	ROM No. State	FOM No. ODEs	ROM No. ODEs
Condenser	75	34	75	53
Evaporator	75	32	75	53

### 4.2.5 Chiller System

The reduced order condenser and evaporator models were coupled with the quasi-static models of the compressor and TXV, and the controller model to form a reduced cycle model. The model was implemented in Dymola, which provides a user-friendly graphical interface for model composition. Fig. 4.12 shows the cycle model diagram. Each component was modeled by equations described earlier, and connectors were constructed for the corresponding models. As shown in the figure, the four major components are connected by connectors having the refrigerant pressure, enthalpy as potential variables, and mass flow rates as flow variables. Connectors connecting the evaporator, bulb, and TXV are composed of temperatures as potential variables. Finally, the water temperature at the evaporator outlet is fed into the controller model, whose output, the control signal, is sent to the compressor. After building component models and defining connectors, components are connected by drawing connections between connectors. The controller was modeled by a discrete block, and other components were implemented as equation-based models.

### 4.3 Initial Conditions and Control Inputs

Finding consistent initial conditions for solving the system of DAEs is a difficult issue in dynamic VCC modeling [2]. Good initial guesses are critical for model convergence and efficiency. Typically initialization of heat exchanger models is completed by solving the over-determined steady-state system with user-defined constraints. In this work, the standard finite volume models applying refrigerant pressure and enthalpies as states were solved first to obtain the enthalpy profile along the heat exchanger. Then density and internal energy of each control volume was calculated from it. Since the system is initialized at a steady-state condition, simulating the model with fixed boundary conditions yields consistent initialization for the transient simulation.

The control inputs to the cycle model consist of condenser and evaporator water inlet temperatures and mass flow rates, and the chilled water temperature set point.

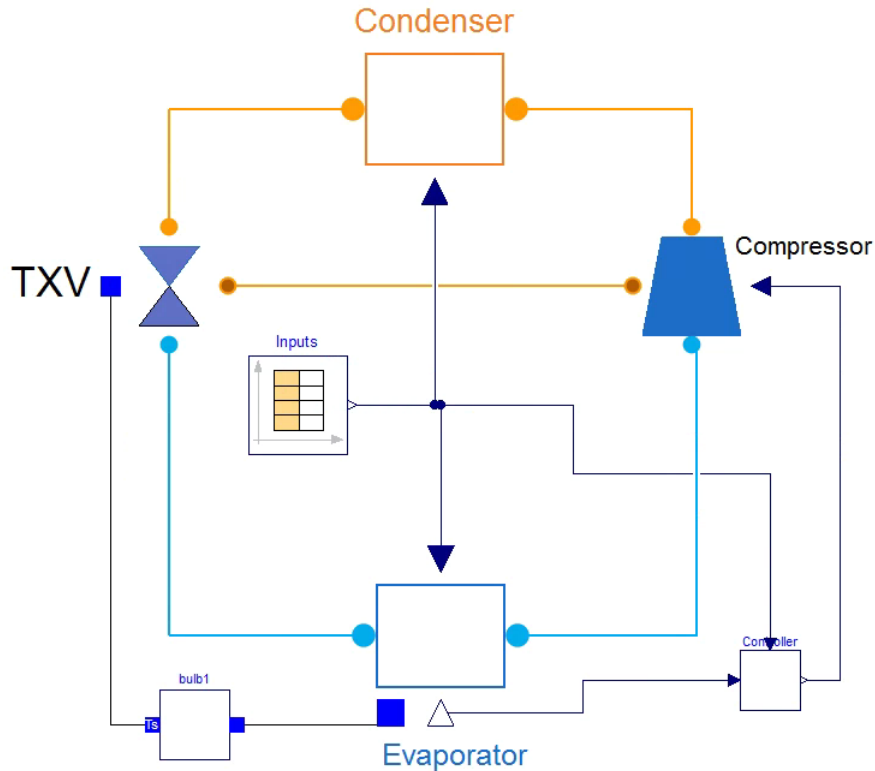


Fig. 4.12. chiller system model implemented in Dymola.

A sequence of 26 operating conditions of the chiller system are considered. Changes of condenser and evaporator water inlet temperatures as well as the the set point temperature are shown in Fig. 4.13. Changes of water inlet mass flow rates are shown in Fig. 4.14.

#### 4.4 Load-change Transients

The reduced order cycle model was simulated to predict cycle transient responses of 26 operating conditions, and was compared with measurements to validate the proposed approach. The primary goal of developing reduced order VCC models is to facilitate control and FDD design, or equipment optimizations. Based on these purposes, it is of more interest in modeling the load-change transients than the start-

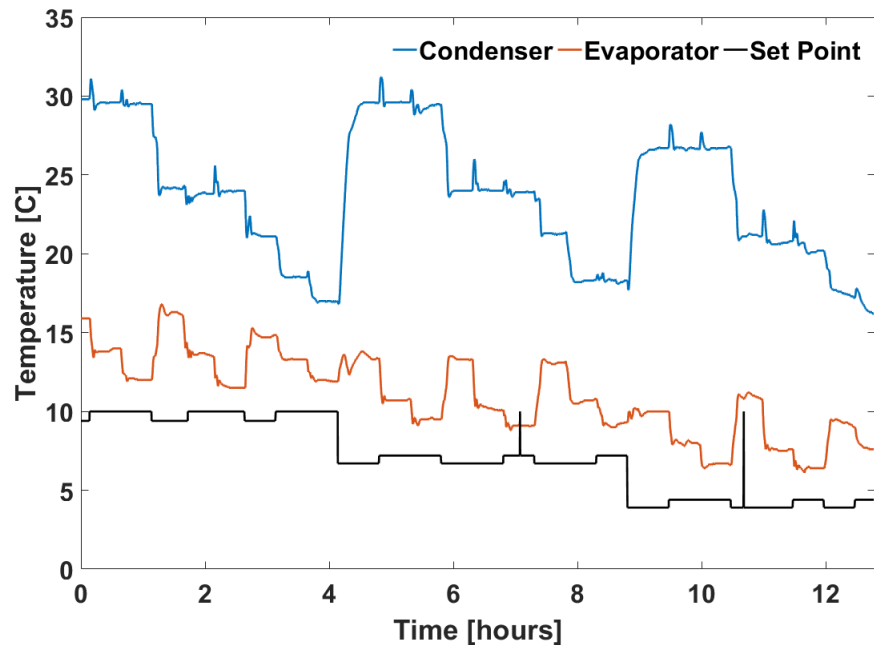


Fig. 4.13. Control inputs of water inlet temperatures and set point temperature.

up for chiller applications, because the start-up or shut-down do not appear often. For a feasibility demonstration, the reformulated full order model was used to predict the start-up transients, and was compared with experimental data. The results are presented in Appendix.

Note that the reduced order condenser and evaporator models were generated based on system responses around the first four operating conditions, and for the rest of 22 operating conditions, their control inputs and trajectories are completely new to the reduced order models. Fig. 4.15 - 4.20 show the pressures, water exit temperatures, motor power, heat exchanger load and the refrigerant liquid mass flow rate (on the TXV side) predictions of the POD-DEIM reduced order model during the complete operation of 12.8 hours run time along the 26 operating conditions. The system was initialized at the first operating condition. Results are compared with the reformulated full order model (FOM), the standard FV model utilizing refrigerant pressure and enthalpy as states (FV\_Ph), and measurements. In Fig.

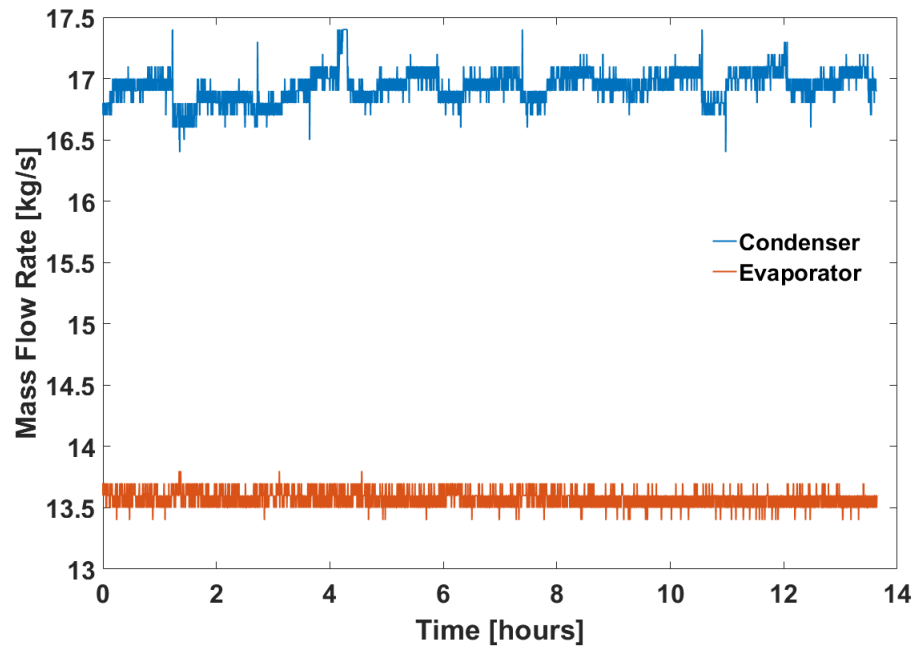


Fig. 4.14. Control inputs of water mass flow rates.

4.15, to the left of the vertical dashed line shows the four operating conditions used for generating the reduced order models (POD-DEIM), thus the results represent reproduction of system responses by the reduced order system from the snapshots. To the right are the 22 operating conditions that the reduced order model had never seen before, and it indicates the generalization ability of the reduced order model. The prediction accuracies of the reformulated full order model and the standard FV model are nearly identical, and agree well with the measurements. The differences between predictions of the reduced order model and the measurements are typically seen for the 22 operating conditions that the reduced order model have never seen. This is because the reduced bases were constructed based on limited information of the system dynamics, and the snapshots have never explored the state space and input space corresponding to these operating conditions. However, the reduced order model is still capable of capturing the dominant dynamics of the chiller system. Transient

prediction errors were quantified by the normalized error residual (NER) [4] computed by:

$$\text{NER} = \frac{\sum_{k=1}^t (y_{\text{predicted}}(k) - y_{\text{measured}}(k))^2}{\sum_{k=1}^t (y_{\text{measured}}(k))^2} \quad (4.22)$$

where  $y_{\text{predicted}}(k)$  denotes the prediction and  $y_{\text{measured}}(k)$  denotes the measurement at the time step  $k$ . NER of refrigerant pressures, water exit temperatures, heat exchanger loads, liquid refrigerant mass flow rate and motor power throughout the load-change transients were computed and shown in Fig. 4.21. It can be seen that all transient prediction errors lie below 0.025. Relatively high errors occurred in predictions of the condenser load, refrigerant flow rate and motor power, while others within 0.002. Transient agreement with the measurements indicates the generalization ability of the reduced order model. Fig. 4.22-4.24 shows the steady-state predictions of the refrigerant pressures, water exit temperatures and cooling (evaporator) loads. It is seen that steady-state predictions agree well with the measured data with prediction errors within 5% for pressures and cooling loads, and within 1°C for water exit temperatures.

#### 4.5 Simulation Speed

The simulation speed is measured by the real time factor (RTF) [4]:

$$\text{RTF} = \frac{\textit{length of time taken to run simulation}}{\textit{length of time that is simulated}}. \quad (4.23)$$

For practical uses like real-time simulation or testing, a model having RTF less than 1 is usually required. Simulation speeds of the POD-DEIM reduced cycle model, the full order model, and the standard FV model are shown in Table 4.3. The number of dynamic states as well as number of ODEs needed to be solved of each model are also displayed, since they play an important role in determining the model execution speed. It is clear that these models all run faster than the real time. The reformulated FV model is more than 2 times faster than the standard FV model in descriptor form, and the reduced order model is more than 2 times faster than the reformulated full order model, and it executes 200 times faster than real time.

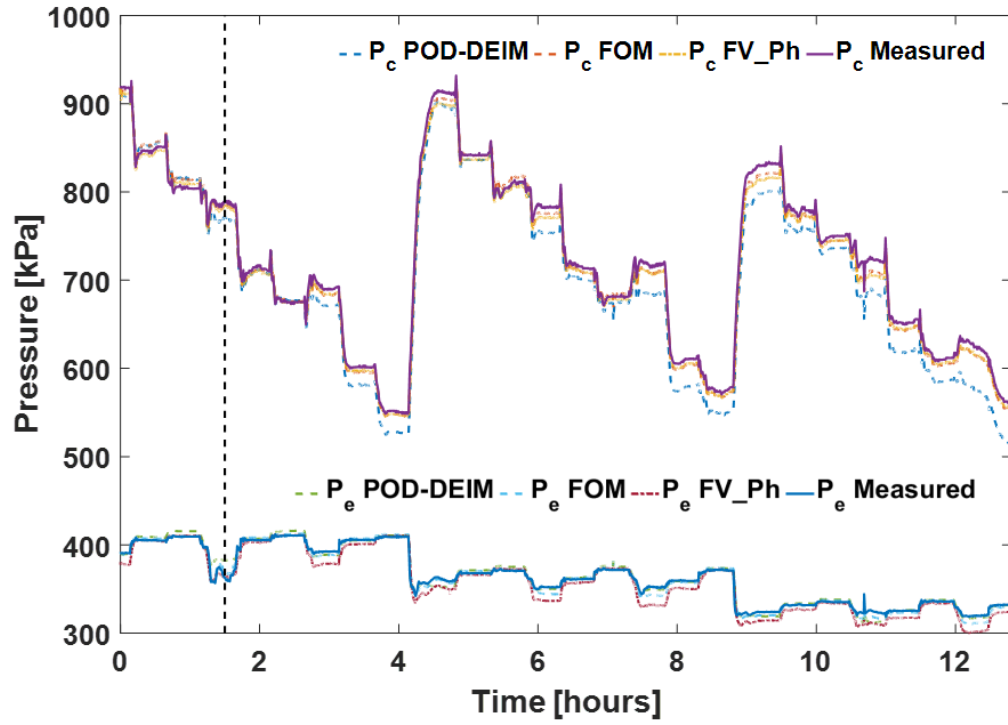


Fig. 4.15. Condensing and evaporating pressures.

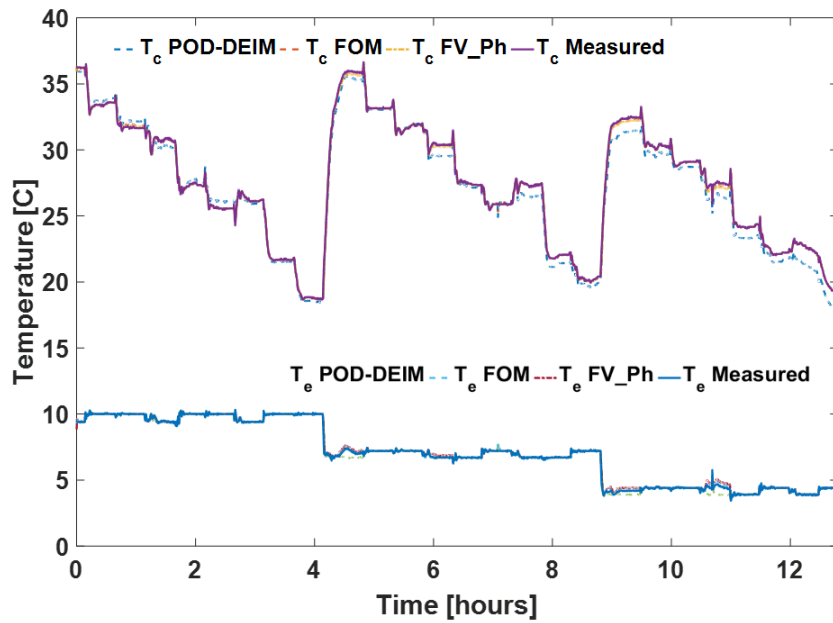


Fig. 4.16. Condenser and evaporator water exit temperatures.

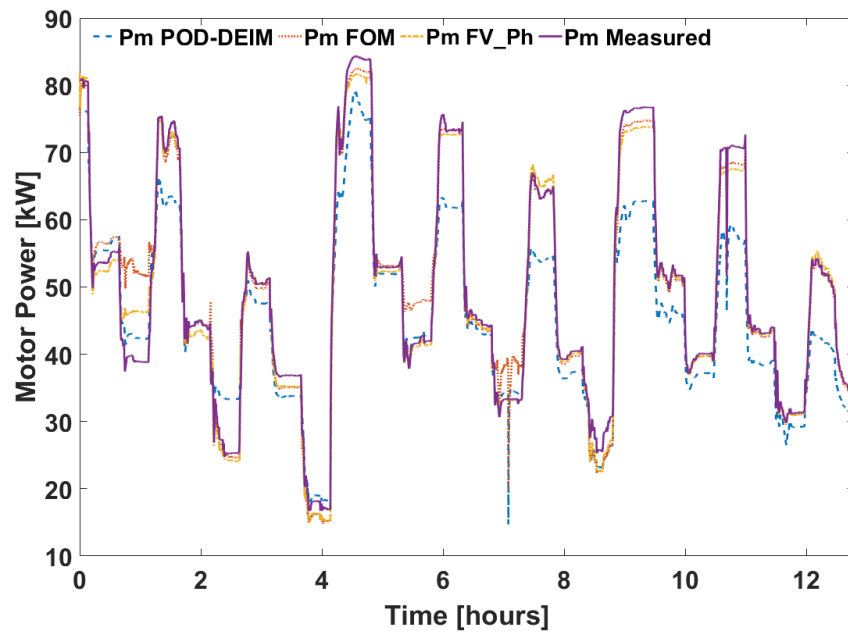


Fig. 4.17. Motor Power.

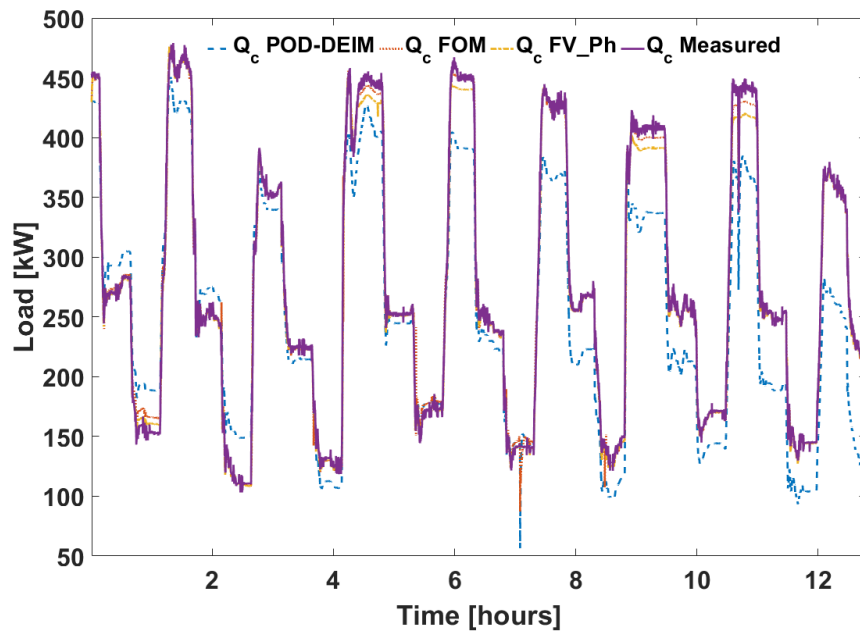


Fig. 4.18. Condenser load.

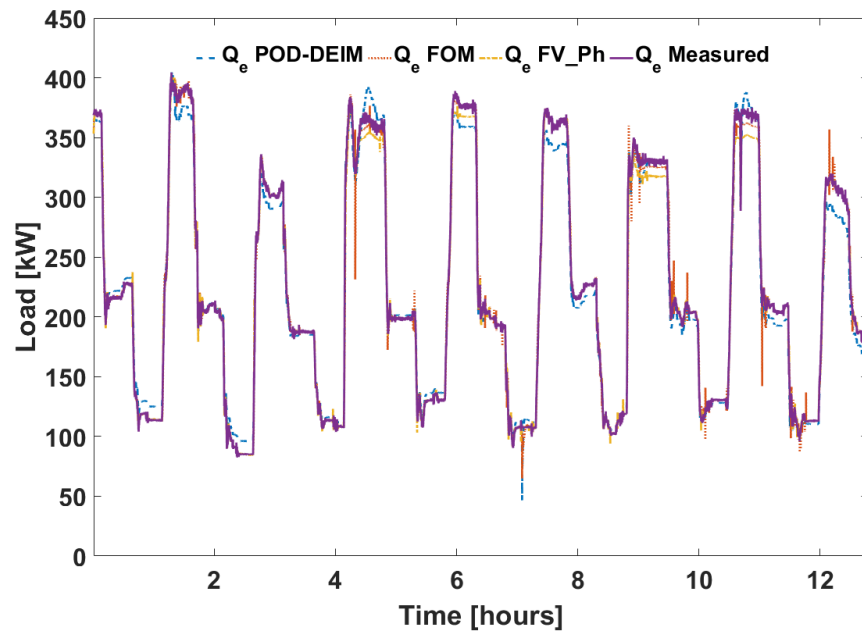


Fig. 4.19. Evaporator load.

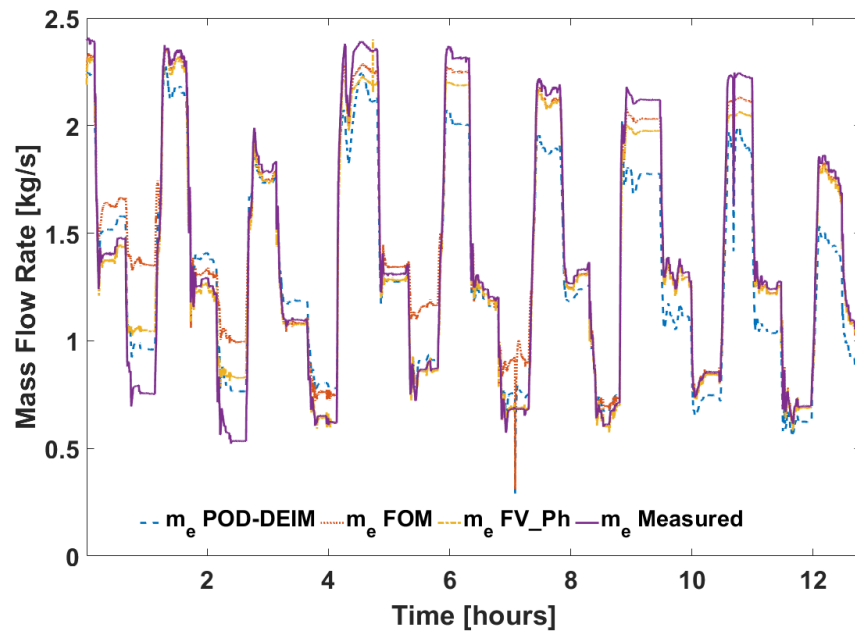


Fig. 4.20. Liquid refrigerant mass flow rate.

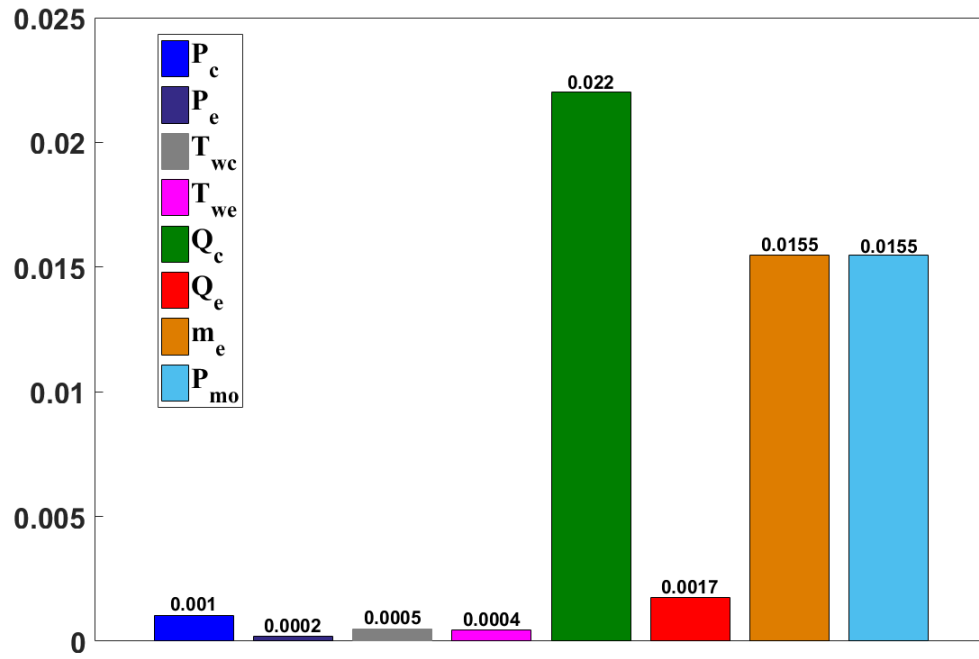


Fig. 4.21. Normalized Error Residual.

It is observed that though the reformulated full order model consists of more states and evaluates a larger set of ODEs, it executes much faster than the standard FV model. For numerical integration of dynamical systems, the solver should first

Table 4.3.  
Simulation speed comparison

Simulation	No. States	No. ODEs	RTF
Standard FV (P,h)	92	92	0.03
Reformulated FOM	150	150	0.0137
POD-DEIM ROM	66	106	0.005

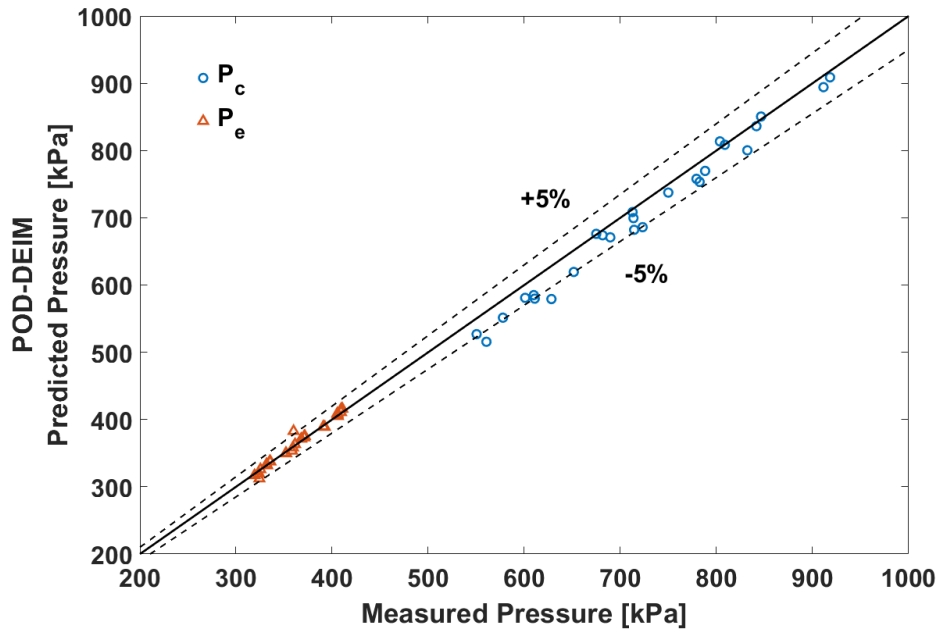


Fig. 4.22. Steady-state condensing and evaporating pressures.

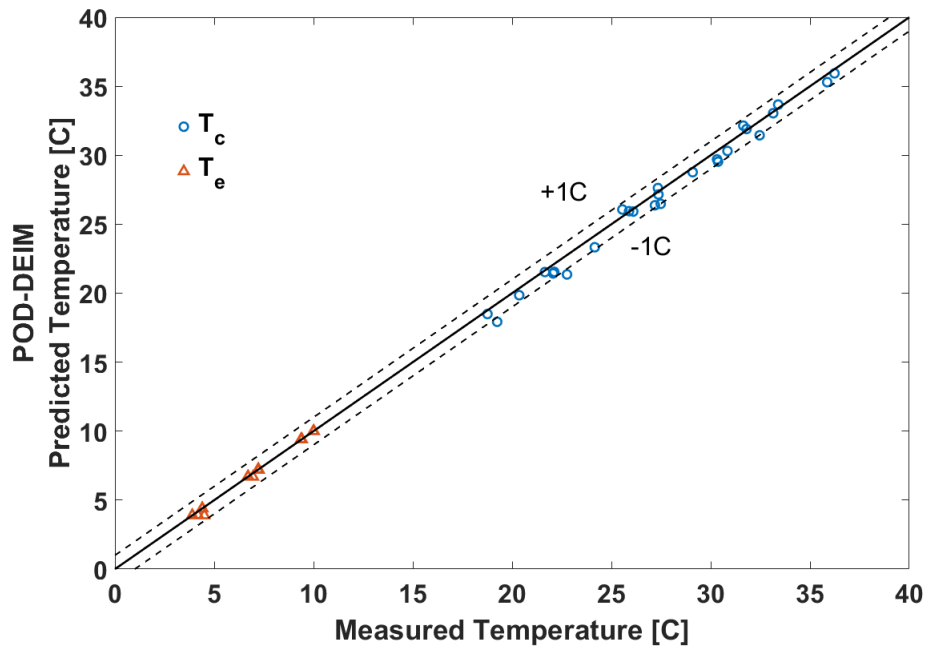


Fig. 4.23. Steady-state exit water temperatures.

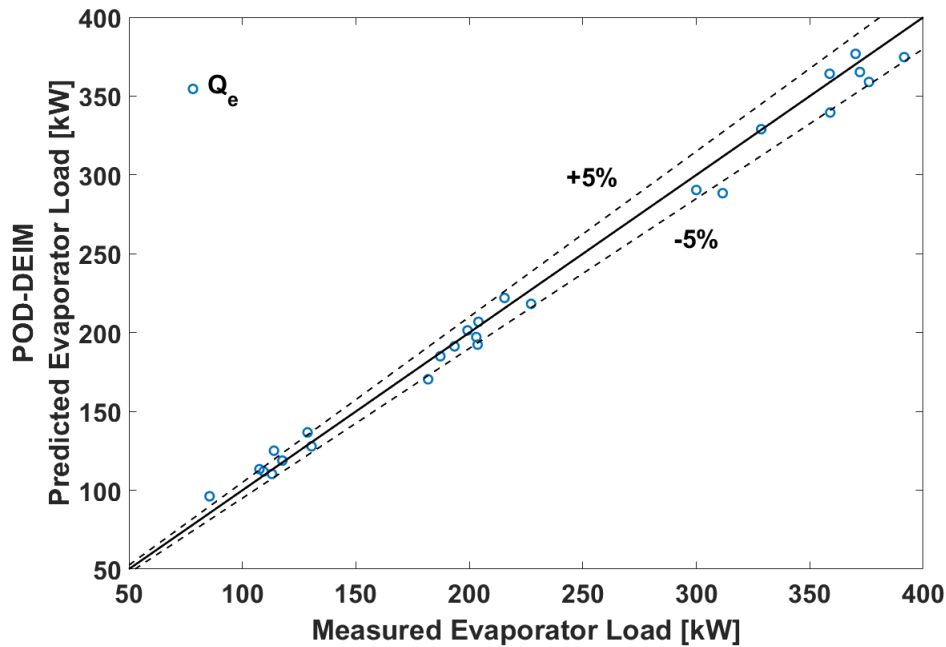


Fig. 4.24. Steady-state evaporator loads.

transform the system to an explicit form, which is the standard ODE structure. Solving the FV model in the descriptor form involves matrix inverse operation at every time step, and this process is usually computationally expensive. Another explanation for this phenomena could be the underlying discontinuities in partial derivatives of the refrigerant properties [42]. For example, Fig. 4.25 displays refrigerant density of R134a at 8 bar crossing different phase regions. Here a general refrigerant quality is utilized. Quality extended to be less than 0 represents the liquid phase, and greater than 1 represents the vapor phase. It is clear that the derivative of density to quality is discontinuous at the saturated liquid line ( $x=0$ ). Since refrigerant quality is a function of pressure and enthalpy ( $x = x(P, h)$ ), it should be expected that the partial derivatives of density with respect to pressure and enthalpy are discontinuous at this point. The partial derivatives calculated in the TIL Media package (a commercial refrigerant property library in Modelica) are shown in Fig. 4.26(a) and 4.26(b), which verify the discontinuity. The existence of discontinuities will cause the solver to take

smaller integration time step because of these large values of derivatives, and slow down the simulation as a result.

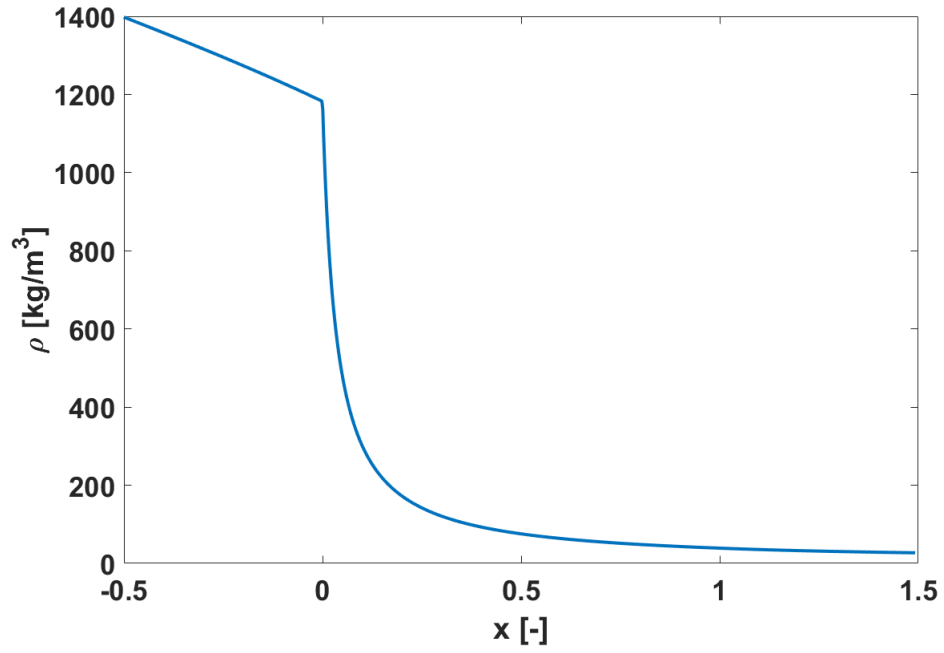
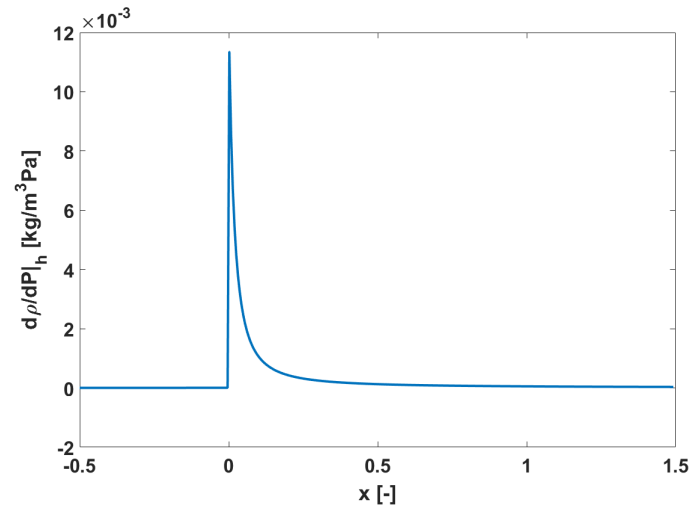
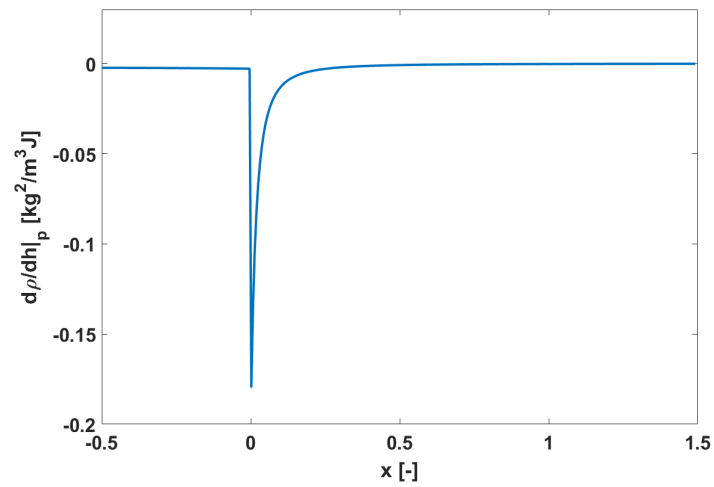


Fig. 4.25. Density of R134a at 8 bar.



(a) Partial derivative of density with respect to pressure of R134a at 8 bar.



(b) Partial derivative of density with respect to enthalpy of R134a at 8 bar.

Fig. 4.26. Density derivatives.

## 5. SUMMARY AND RECOMMENDATIONS

### 5.1 Summary

A nonlinear model order reduction framework for generating reduced order vapor compression cycle models has been developed. This method starts with reformulation of the dynamic finite volume heat exchanger models to the standard ODE structure, by utilizing refrigerant density, internal energy, and interface mass flow rates as dynamic states. The momentum balances are integrated in the governing equations to evaluate dynamics of the interface mass flow rates, and a staggered grid is applied for discretization. Reduced order condenser and evaporator models are constructed by the Proper Orthogonal Decomposition (POD). Due to the high nonlinearity of the heat exchanger models, the reduced order models directly derived from the POD method have a computational complexity issue, though the number of dynamic states is reduced. Therefore, the Discrete Empirical Interpolation Method (DEIM) is applied to approximate the nonlinear functions, and further improve the dimension reduction efficiency. Reduced order condenser and evaporator models are constructed for a centrifugal chiller system. Under the current POD-DEIM model reduction scheme, more than half of the dynamic states of heat exchanger models are reduced, and one third of nonlinear functions are eliminated.

The resulting POD-DEIM reduced order models are coupled with quasi-static models of the compressor and expansion valve to complete the reduced order VCC model. The model was used to predict load-change transients of a chiller, along a sequence of 26 operating conditions. It should be noted that the reduced order heat exchanger models were constructed from four of them, and the remaining 22 operating conditions were not seen by the reduced order models. Validation results of the refrigerant pressures, water exit temperatures, motor power, condenser and evapo-

rator loads and the refrigerant mass flow rate were compared with the reformulated full order model, the standard finite volume model applying the refrigerant pressure and enthalpies as states, as well as the measurements. Agreement between predictions and measurements indicates the generalization ability of the proposed MOR approach and that the reduced order model accurately captures the dynamics of the VCC system. Furthermore, steady-state predictions of pressures, cooling loads and water exit temperatures agree well with the measured data with prediction errors within 5% and 1°C.

The simulation speed comparisons reveal that the full order reformulated model is more than 2 times faster than the standard FV model, and the reduced order model is more than 2 times faster than the full order model with negligible approximation error. The reduced VCC model executes 200 times faster than the real time, and could be directly used for control and fault detection applications.

## 5.2 Recommendations

To the best of the author’s knowledge, this work is the first attempt for constructing nonlinear reduced order VCC models, and conducting validations. The validations for a chiller system indicate that the reduced order model is capable of capturing dynamics of the VCC system, and can save significant computation time with relatively small prediction errors. This work can be considered as a feasibility study. To further demonstrate generalization of the proposed model order reduction approach, additional validations could be conducted on an air-cooled VCC system, e.g. a rooftop air conditioner, which implies different dynamics than a chiller. Other applications of reduced order VCC models include dynamic modeling of variable refrigerant flow (VRF) systems with multiple indoor units, heat pumps or refrigerators with frost formation and defrost applications.

Even though the proposed POD-DEIM model reduction framework demonstrated great applicability in reducing computational time for transient VCC simulations, the

global stability of the reduced order model is not guaranteed for every combination of control inputs. The current approach stabilizes the reduced order models at some equilibrium points by linearizing the full order models. Therefore, only local stability near these equilibrium points are taken care of. It is possible that the system becomes unstable for a state space that the reduced order model has never seen. Since directly stabilizing nonlinear systems is very challenging [53, 54], an alternative model order reduction approach for nonlinear systems could be developed based on linearized models. For example, the trajectory piecewise-linear (TPWL) method approximates nonlinear dynamical systems by pieces of linearized models generated along a state trajectory [55, 56]. Then each piece can be reduced by model order reduction techniques to obtain a reduced order system. Note that each piece is a linear time-invariant (LTI) system, which can be stabilized by existing approaches (such as those mentioned in this thesis), and once they are stabilized, the resulting system is guaranteed to be stable for any control inputs.

Other nonlinear model order reduction methods are worthy of investigation for vapor compression systems. The POD method concentrates on approximation of the controllability grammain, and captures the system dynamics without consideration of the relationship between states and outputs. In some cases, it may fail to accurately represent system outputs. To overcome this problem, the Balanced Proper Orthogonal Decomposition (BPOD) and the Empirical Balanced Truncation (EBT) methods, which take into account both the system controllability and observability, may be applied to produce high-fidelity output quantities.

## REFERENCES

## REFERENCES

- [1] B. P. Rasmussen and A. G. Alleyne, “Dynamic modeling and advanced control of air conditioning and refrigeration systems,” Air Conditioning and Refrigeration Center. College of Engineering . . . , Tech. Rep., 2006.
- [2] M. Wetter, “Modelica-based modelling and simulation to support research and development in building energy and control systems,” *Journal of Building Performance Simulation*, vol. 2, no. 2, pp. 143–161, 2009.
- [3] M. C. Keir and A. G. Alleyne, “Dynamic modeling, control, and fault detection in vapor compression systems,” Air Conditioning and Refrigeration Center. College of Engineering . . . , Tech. Rep., 2006.
- [4] H. Pangborn, A. G. Alleyne, and N. Wu, “A comparison between finite volume and switched moving boundary approaches for dynamic vapor compression system modeling,” *International Journal of Refrigeration*, vol. 53, pp. 101–114, 2015.
- [5] S. Bendapudi, J. E. Braun, and E. A. Groll, “A comparison of moving-boundary and finite-volume formulations for transients in centrifugal chillers,” *International journal of refrigeration*, vol. 31, no. 8, pp. 1437–1452, 2008.
- [6] A. Desideri, B. Dechesne, J. Wronski, M. Van den Broek, S. Gusev, V. Lemort, and S. Quoilin, “Comparison of moving boundary and finite-volume heat exchanger models in the modelica language,” *Energies*, vol. 9, no. 5, p. 339, 2016.
- [7] H. Qiao, C. R. Laughman, V. Aute, and R. Radermacher, “An advanced switching moving boundary heat exchanger model with pressure drop,” *International Journal of Refrigeration*, vol. 65, pp. 154–171, 2016.
- [8] J. W. MacArthur, “Transient heat pump behaviour: a theoretical investigation,” *International Journal of Refrigeration*, vol. 7, no. 2, pp. 123–132, 1984.
- [9] W.-D. Gruhle and R. Isermann, “Modeling and control of a refrigerant evaporator,” in *1985 American Control Conference*. IEEE, 1985, pp. 287–292.
- [10] S. Bendapudi, *Development and evaluation of modeling approaches for transients in centrifugal chillers*. Purdue University, 2004.
- [11] C. Tso, Y. Cheng, and A. Lai, “Dynamic behavior of a direct expansion evaporator under frosting condition. part i. distributed model,” *International journal of refrigeration*, vol. 29, no. 4, pp. 611–623, 2006.
- [12] W.-J. Zhang, C.-L. Zhang, and G.-L. Ding, “On three forms of momentum equation in transient modeling of residential refrigeration systems,” *International Journal of Refrigeration*, vol. 32, no. 5, pp. 938–944, 2009.

- [13] E. W. Grald and J. W. MacArthur, “A moving-boundary formulation for modeling time-dependent two-phase flows,” *International Journal of Heat and Fluid Flow*, vol. 13, no. 3, pp. 266–272, 1992.
- [14] X.-D. He, “Dynamic modeling and multivariable control of vapor compression cycles in air conditioning systems,” Ph.D. dissertation, Massachusetts Institute of Technology, 1996.
- [15] B. P. Rasmussen and A. G. Alleyne, “Control-oriented modeling of transcritical vapor compression systems,” *J. Dyn. Sys., Meas., Control*, vol. 126, no. 1, pp. 54–64, 2004.
- [16] M. Willatzen, N. Pettit, and L. Ploug-Sørensen, “A general dynamic simulation model for evaporators and condensers in refrigeration. part i: moving-boundary formulation of two-phase flows with heat exchange: Modèle général dynamique pour évaporateurs et condenseurs frigorifiques. partie i: Formulation des conditions aux limites variables de flux biphasiques avec échange de chaleur,” *International Journal of refrigeration*, vol. 21, no. 5, pp. 398–403, 1998.
- [17] J. M. Jensen and H. Tummescheit, “Moving boundary models for dynamic simulations of two-phase flows,” in *Proc. of the 2nd int. modelica conference*, vol. 3. Oberpfaffenhofen Germany, 2002.
- [18] W.-J. Zhang and C.-L. Zhang, “A generalized moving-boundary model for transient simulation of dry-expansion evaporators under larger disturbances,” *International Journal of Refrigeration*, vol. 29, no. 7, pp. 1119–1127, 2006.
- [19] T. L. McKinley and A. G. Alleyne, “An advanced nonlinear switched heat exchanger model for vapor compression cycles using the moving-boundary method,” *International Journal of refrigeration*, vol. 31, no. 7, pp. 1253–1264, 2008.
- [20] B. P. Rasmussen, “Dynamic modeling for vapor compression systems—part i: Literature review,” *HVAC&R Research*, vol. 18, no. 5, pp. 934–955, 2012.
- [21] P. Li, H. Qiao, Y. Li, J. E. Seem, J. Winkler, and X. Li, “Recent advances in dynamic modeling of hvac equipment. part 1: Equipment modeling,” *HVAC&R Research*, vol. 20, no. 1, pp. 136–149, 2014.
- [22] P. Li, Y. Li, J. E. Seem, H. Qiao, X. Li, and J. Winkler, “Recent advances in dynamic modeling of hvac equipment. part 2: Modelica-based modeling,” *HVAC&R Research*, vol. 20, no. 1, pp. 150–161, 2014.
- [23] M. Wetter, W. Zuo, and T. S. Noudui, “Recent developments of the modelica” buildings” library for building energy and control systems,” Lawrence Berkeley National Lab.(LBNL), Berkeley, CA (United States), Tech. Rep., 2011.
- [24] X.-D. He, S. Liu, H. H. Asada, and H. Itoh, “Multivariable control of vapor compression systems,” *HVAC&R Research*, vol. 4, no. 3, pp. 205–230, 1998.
- [25] N. Jain, D. J. Burns, S. Di Cairano, C. R. Laughman, and S. Bortoff, “Model predictive control of vapor compression systems,” in *15th International Refrigeration and Air Conditioning Conference at Purdue*, 2014.

- [26] B. Li, N. Jain, and A. G. Alleyne, “Lmi control design for nonlinear vapor compression cycle systems,” in *ASME 2012 5th Annual Dynamic Systems and Control Conference joint with the JSME 2012 11th Motion and Vibration Conference*. American Society of Mechanical Engineers, 2012, pp. 711–718.
- [27] S. Chaturantabut and D. C. Sorensen, “Nonlinear model reduction via discrete empirical interpolation,” *SIAM Journal on Scientific Computing*, vol. 32, no. 5, pp. 2737–2764, 2010.
- [28] P. A. LeGresley, *Application of proper orthogonal decomposition (POD) to design decomposition methods*. Stanford University, 2006.
- [29] G. Kerschen, J.-c. Golinval, A. F. Vakakis, and L. A. Bergman, “The method of proper orthogonal decomposition for dynamical characterization and order reduction of mechanical systems: an overview,” *Nonlinear dynamics*, vol. 41, no. 1-3, pp. 147–169, 2005.
- [30] G. Berkooz, P. Holmes, and J. L. Lumley, “The proper orthogonal decomposition in the analysis of turbulent flows,” *Annual review of fluid mechanics*, vol. 25, no. 1, pp. 539–575, 1993.
- [31] K. C. Hall, J. P. Thomas, and E. H. Dowell, “Proper orthogonal decomposition technique for transonic unsteady aerodynamic flows,” *AIAA journal*, vol. 38, no. 10, pp. 1853–1862, 2000.
- [32] K. Kunisch and S. Volkwein, “Control of the burgers equation by a reduced-order approach using proper orthogonal decomposition,” *Journal of optimization theory and applications*, vol. 102, no. 2, pp. 345–371, 1999.
- [33] J. Berger, S. Guernouti, and M. Woloszyn, “Evaluating model reduction methods for heat and mass transfer in porous materials: Proper orthogonal decomposition and proper generalized decomposition,” *Journal of Porous Media*, vol. 22, no. 3, 2019.
- [34] S. Prajna, “Pod model reduction with stability guarantee,” in *42nd IEEE International Conference on Decision and Control (IEEE Cat. No. 03CH37475)*, vol. 5. IEEE, 2003, pp. 5254–5258.
- [35] D. Amsallem and C. Farhat, “Stabilization of projection-based reduced-order models,” *International Journal for Numerical Methods in Engineering*, vol. 91, no. 4, pp. 358–377, 2012.
- [36] B. B. King and E. W. Sachs, “Semidefinite programming techniques for reduced order systems with guaranteed stability margins,” *Computational Optimization and Applications*, vol. 17, no. 1, pp. 37–59, 2000.
- [37] M. Grant and S. Boyd, “Cvx: Matlab software for disciplined convex programming, version 2.1,” 2014.
- [38] I. Kalashnikova, S. Arunajatesan, M. F. Barone, B. G. van Bloemen Waanders, and J. A. Fike, “Reduced order modeling for prediction and control of large-scale systems,” *Sandia National Laboratories Report, SAND*, no. 2014-4693, 2014.
- [39] J. Chi and D. Didion, “A simulation model of the transient performance of a heat pump,” *International Journal of Refrigeration*, vol. 5, no. 3, pp. 176–184, 1982.

- [40] H. Elmqvist, H. Tummescheit, and M. Otter, “Object-oriented modeling of thermo-fluid systems,” in *Proceedings of the 3rd International Modelica Conference*, 2003.
- [41] C. R. Laughman and H. Qiao, “On closure relations for dynamic vapor compression cycle models,” in *Proceedings of The American Modelica Conference 2018, October 9-10, Somberg Conference Center, Cambridge MA, USA*, no. 154. Linköping University Electronic Press, 2019, pp. 67–76.
- [42] —, “On the influence of state selection on mass conservation in dynamic vapour compression cycle models,” *Mathematical and Computer Modelling of Dynamical Systems*, vol. 23, no. 3, pp. 262–283, 2017.
- [43] C. Junior, C. Richter, W. Tegethoff, N. Lemke, and J. Köhler, “Modeling and simulation of a thermoelectric heat exchanger using the object-oriented library til,” in *Proceedings of the 6th International Modelica Conference*, 2008, pp. 437–445.
- [44] E. W. Lemmon, M. L. Huber, and M. O. McLinden, “Nist reference fluid thermodynamic and transport properties–refprop,” *NIST standard reference database*, vol. 23, p. v7, 2002.
- [45] I. H. Bell, S. Quoilin, J. Wronski, and V. Lemort, “Coolprop: An open-source reference-quality thermophysical property library,” in *ASME ORC 2nd International Seminar on ORC Power Systems*, 2013.
- [46] J. Mannewitz, R. Langebach, and U. Hesse, “Development of a fast method for retrieving thermodynamic properties to accelerate transient vapor compression cycle simulation,” 2018.
- [47] G. Ding, Z. Wu, J. Liu, T. Inagaki, K. Wang, and M. Fukaya, “An implicit curve-fitting method for fast calculation of thermal properties of pure and mixed refrigerants,” *International Journal of Refrigeration*, vol. 28, no. 6, pp. 921–932, 2005.
- [48] C. Laughman, Y. Zhao, and D. Nikovski, “Fast refrigerant property calculations using interpolation-based methods,” 2012.
- [49] A. Alleyne *et al.*, “et. al., “thermosys 4 toolbox,” university of illinois at urbana-champaign,” 2012.
- [50] A. Dassault Systèmes, “Dymola user manual volume 1,” 2014.
- [51] H. Qiao, “Transient modeling of two-stage and variable refrigerant flow vapor compression systems with frosting and defrosting,” Ph.D. dissertation, 2014.
- [52] C. Laughman, H. Qiao, and D. Nikovski, “Kernel regression for the approximation of heat transfer coefficients,” in *Gustav Lorentzen Natural Working Fluids Conference*, 2016.
- [53] R. Pulch, “Stability preservation in galerkin-type projection-based model order reduction,” *arXiv preprint arXiv:1711.02912*, 2017.
- [54] C. Gu, “Model order reduction of nonlinear dynamical systems,” Ph.D. dissertation, UC Berkeley, 2011.

- [55] M. Rewieński and J. White, “Model order reduction for nonlinear dynamical systems based on trajectory piecewise-linear approximations,” *Linear algebra and its applications*, vol. 415, no. 2-3, pp. 426–454, 2006.
- [56] D. Gratton and K. Willcox, “Reduced-order, trajectory piecewise-linear models for nonlinear computational fluid dynamics,” in *34th AIAA Fluid Dynamics Conference and Exhibit*, 2004, p. 2329.

## APPENDIX

## A. START-UP TRANSIENTS PREDICTIONS

The reformulated heat exchanger models were integrated into the cycle model to predict the start-up transient of the chiller system, and was compared with measurements. In addition, results were compared with the standard finite volume models. 15 control volumes are applied for both the reformualted and the standard FV models. The condenser was initialized to a condition of superheated vapor, while the evaporator was initialized to a two-phase condition of thermal equilibrium with the water inlet temperature. The cycle was driven by boundary conditions as shown in Fig. A.1, and the chilled water set point temperature is  $9.4^{\circ}\text{C}$  throughout the start-up period.

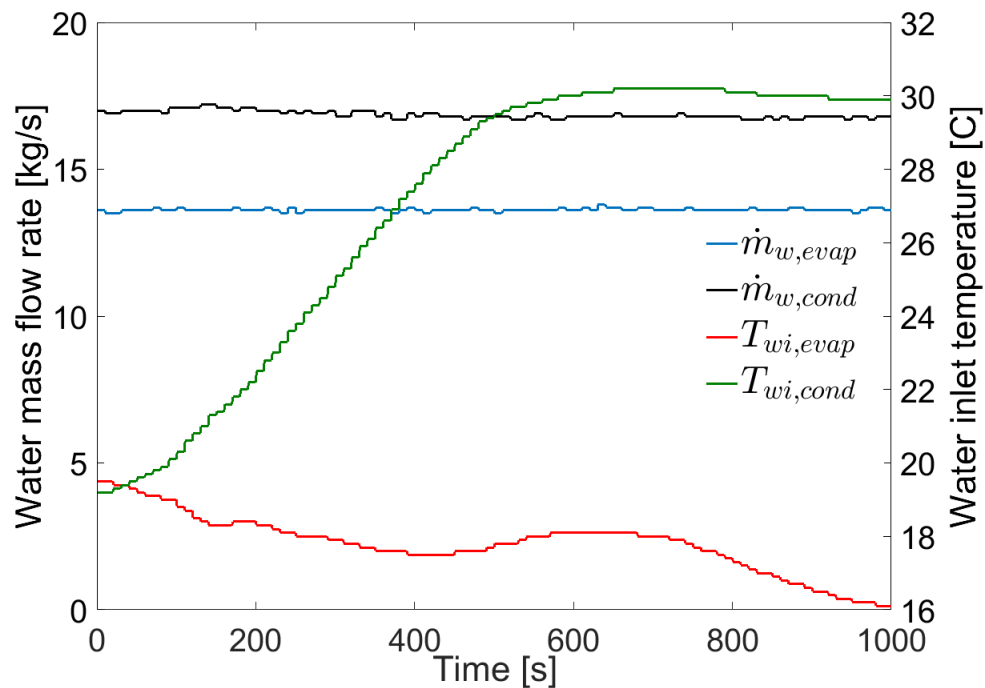


Fig. A.1. Cycle boundary conditions: heat exchanger water mass flow rates and inlet temperatures.

The start-up operation lasted for 1000 seconds, until the chilled water supply temperature reached the set point. Comparisons of the refrigerant pressures, water exit temperatures, heat exchanger loads are presented in Fig. A.2-A.5. The reformulated model is denoted as FV\_ $\rho u$  (using the refrigerant density, internal energy as thermodynamic states), whereas the standard FV model is denoted as FV\_Ph (using the refrigerant pressure and enthalpy as thermodynamic states). Simulation results reveal that the reformulated model agrees very well with the transient experimental data. In terms of simulation speed, the standard FV model has a real time factor of 0.0464, as compared to a value for the reformulated model of 0.0234. With comparable accuracy, the reformulated model executes 2 times faster than the standard FV model.

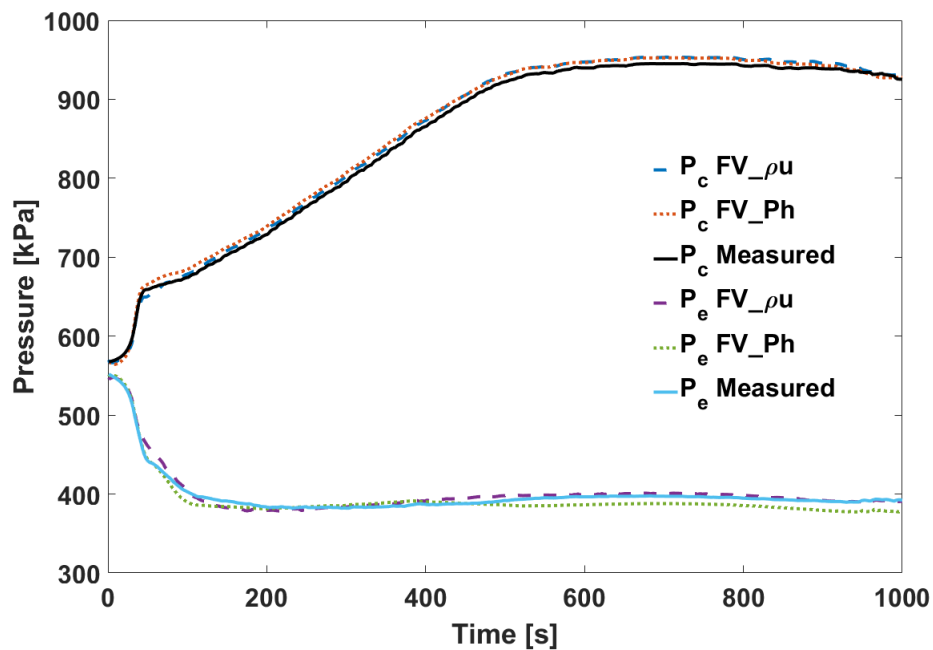


Fig. A.2. Condensing and evaporating pressures

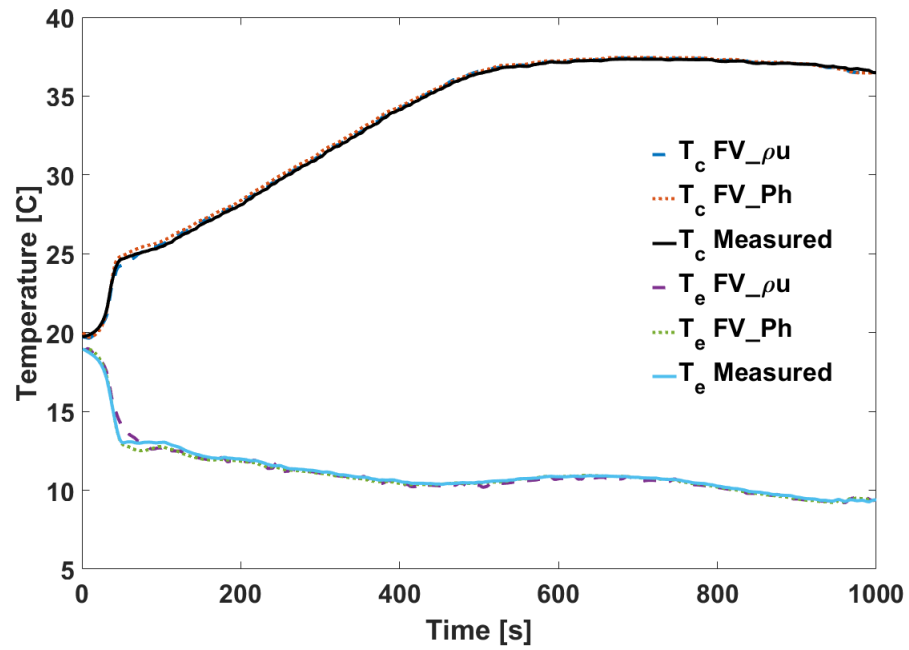


Fig. A.3. Condenser and evaporator water exit temperatures

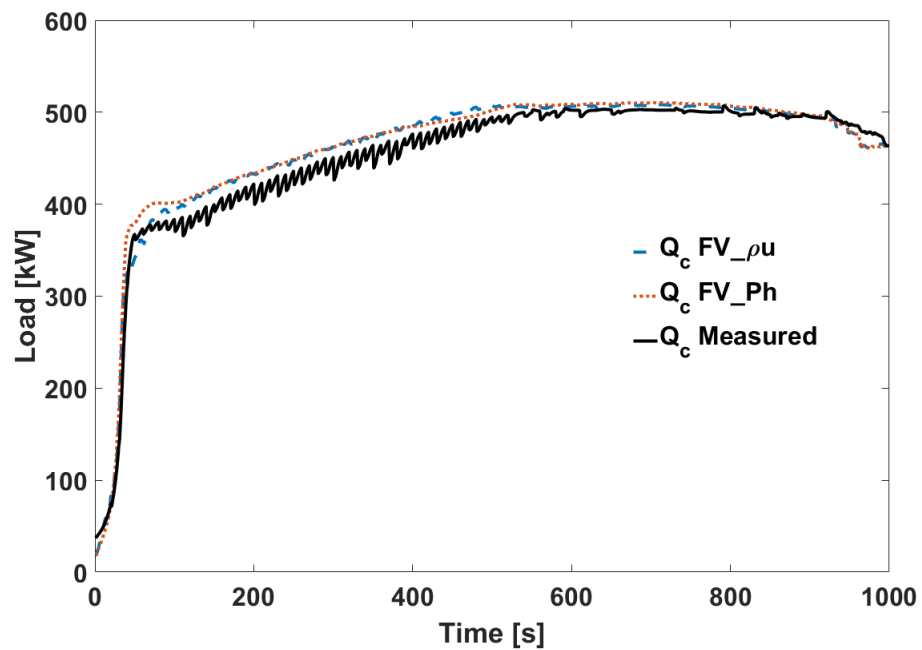


Fig. A.4. Condenser Load.

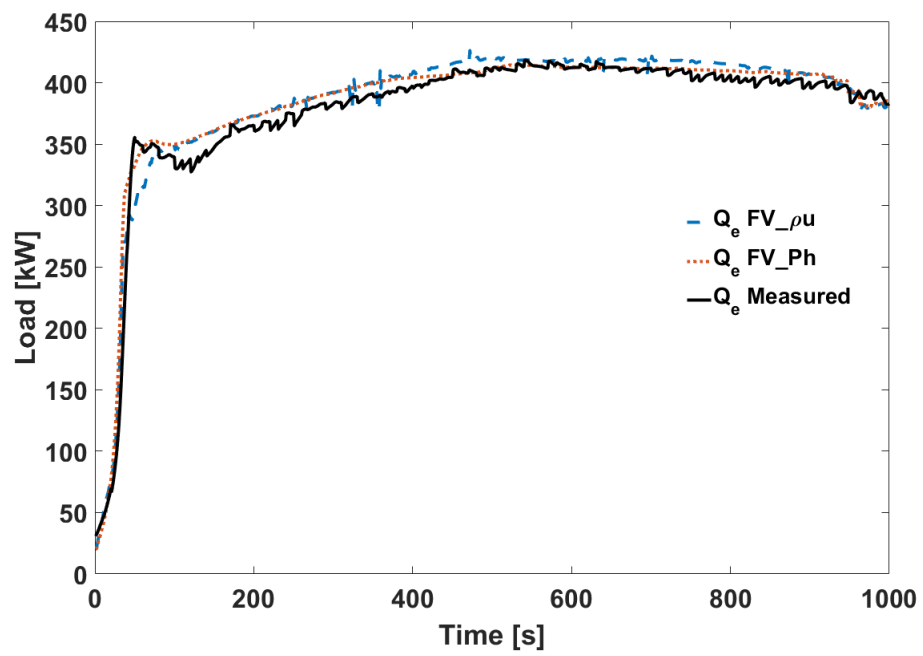


Fig. A.5. Evaporator Load.